UNIVERSIDADE FEDERAL DE PERNAMBUCO
CENTRO DE TECNOLOGIA E GEOCIÊNCIAS
DEPARTAMENTO DE ENGENHARIA CARTOGRÁFICA
PROGRAMA DE PÓS-GRADUAÇÃO EM CIÊNCIAS GEODÉSICAS E TECNOLOGIAS DA GEOINFORMAÇÃO

ABSALÃO ARANHA NASCIMENTO

SPACE-BORNE GNSS RADIO OCCULTATION: validation and analysis of the observed tropopause over South America

Recife
2019

ABSALÃO ARANHA NASCIMENTO

SPACE-BORNE GNSS RADIO OCCULTATION: validation and analysis of the observed tropopause over South America

Dissertation presented to the Graduate Program in Geodetic Sciences and Technologies of Geoinformation, Federal University of Pernambuco, as part of the requirements for obtaining a Master's degree in Geodetic Sciences and Geoinformation Technologies.

Area of concentration: Geodetic Sciences and Geoinformation Technologies.

Advisor: Profº. Dr. Rodrigo Mikosz Gonçalves.

Co-Advisor: Profº. Dr. Joseph Awange.

Recife

2019

Catalogação na fonte
Bibliotecária Maria Luiza de Moura Ferreira, CRB-4 / 1469

N244s Nascimento, Absalão Aranha.
Space-borne GNSS radio occultation: validation and analysis of the observed tropopause over South America / - 2019.
58 folhas, il., tab., abr., sigl. e símb.

Orientador: Prof. Dr. Rodrigo Mikosz Gonçalves.
Coorientador: Prof. Dr. Joseph Awange.

Dissertação (Mestrado) – Universidade Federal de Pernambuco. CTG. Programa de Pós-Graduação em Engenharia Cartográfica, 2019.
Inclui Referências.

1. Engenharia Cartográfica. 2. GNSS-RO. 3. Tropopausa. 4. Teleconexões. 5. América do Sul. I. Gonçalves, Rodrigo Mikosz (Orientador). II. Awange, Joseph (Coorientador). III. Título.

UFPE

621.3 CDD (22. ed.) BCTG/2019-077

ABSALÃO ARANHA NASCIMENTO

SPACE-BORNE GNSS RADIO OCCULTATION:
VALIDATION AND ANALYSIS OF THE OBSERVED TROPOPAUSE OVER SOUTH AMERICA

Dissertation presented to the Graduate Program in Geodetic Sciences and Technologies of Geoinformation, Federal University of Pernambuco, as part of the requirements for obtaining a Master's degree in Geodetic Sciences and Geoinformation Technologies.

Approved in: _20_/_02_/_2019_.

BANCA EXAMINADORA

_____
Profº. Dr. Rodrigo Mikosz Gonçalves (Orientador)
Universidade Federal de Pernambuco

_____
Profª. Drª. Andrea de Seixas (Examinadora Interna)
Universidade Federal de Pernambuco

_____
Profº. Dr. Vagner Gonçalves Ferreira (Examinador Externo)
Universidade Hohai, China

I dedicate this work to my parents, my sisters and my wife, who have supported and encouraged me on this journey.

ACKNOWLEDGMENT

To my family, my parents who believed in me and supported me all these years, to my sisters who have always helped and encouraged me during the realization of this dream;

To my wife for encouraging me and accompanying this trajectory.

To Profº. Dr. Rodrigo Mikosz Gonçalves for guidance, encouragement and kindness in sharing his knowledge.

To the Graduate Program in Geodetic Sciences and Technologies of Geoinformation of the Federal University of Pernambuco.

To the Federal Institute of Espírito Santo, Campus Nova Venécia, which gave me the opportunity to perform the master's degree.

ABSTRACT

Global and regional tropopause monitoring (temperature and height) has taking advantage of atmospheric remote sensing using Global Navigation Satellite System - Radio Occultation (GNSS-RO). In this study, 622,914 GNSS-RO data observations obtained by CHAMP (Challenging Minisatellite Payload), GRACE (Gravity Recovery and Climate Experiment) and COSMIC (Constellation Observing System for Meteorology Ionosphere & Climate), considering 200 months (2001 to 2017) were used to analyze the variability of the height and temperature of the Lapse-Rate Tropopause (LRT) over South America. Firstly the atmospheric profiles were validated using atmospheric observations for 54 radiosonde stations. The results considering South America showed a new trend of 13.450 ± 0.677 meters per decade for the tropopause height which indicates a regional tropopause increase and a corresponding temperature decrease of -0.021 ± 0.002K per decade. The PCA (Principal Component Analysis) of the anomalies of temperature and height of the tropopause presented a significant correlation of 0.60 of the variability of the tropopause with the ENSO (El Niño–Southern Oscillation) phenomenon. The detected increase of tropopause height in South America revel warming evidence that should be monitored.

Keywords: GNSS-RO. Tropopause. Teleconnections. South America.

RESUMO

O monitoramento global e regional de tropopausa (temperatura e altura) tem aproveitado o sensoriamento remoto atmosférico usando o Sistema Global de Navegação por Satélite - Radio Occultation (RO-GNSS). Neste estudo, 622914 observações de dados GNSS-RO obtidas por CHAMP (Challenging Minisatellite Payload), GRACE (Gravity Recovery and Climate Experiment) e COSMIC (Constellation Observing System for Meteorology Ionosphere & Climate), considerando 200 meses (2001 a 2017) foram utilizados para analisar a variabilidade da altura e temperatura da Lapse-Rate Tropopausa (LRT) sobre a América do Sul. Primeiramente, os perfis atmosféricos foram validados utilizando observações atmosféricas para 54 estações de radiossondas. Os resultados, considerando a América do Sul, mostraram uma nova tendência de 13,450 ± 0,677 metros por década para a altura da tropopausa, o que indica um aumento regional da tropopausa e uma diminuição correspondente na temperatura de -0.021 ± 0.002K por década. A PCA (Análise de Componentes Principais) das anomalias de temperatura e altura da tropopausa apresentou correlação significativa de 0,60 da variabilidade da tropopausa com o fenômeno ENSO (El Niño - Oscilação Sul). O aumento detectado da altura da tropopausa na América do Sul revela uma evidência de aquecimento que deve ser monitorada.

Palavras-chave: GNSS-RO. Tropopausa. Teleconexões. América do Sul.

LIST OF FIGURES

LIST OF TABLES

LIST OF ABBREVIATIONS AND ACRONYMS

CDAAC	COSMIC DATA ANALYSIS AND ARCHIVE CENTER
CHAMP	CHALLENGING MINISATELLITE PAYLOAD
COSMIC	CONSTELLATION OBSERVING SYSTEM FOR METEOROLOGY IONOSPHERE & CLIMATE
DLR	DEUTSCHE FORSCHUNGSANSTALT FÜR LUFT UND RAUMFAHRT
ENSO	EL NIÑO SOUTHERN OSCILLATION
EOF	EMPIRICAL ORTHOGONAL FUNCTIONS
EQUARS	EQUATORIAL ATMOSPHERE RESEARCH SATELLITE
FY-3C	FENG-YUN 3C
GFZ	GEOFORSCHUNGSZENTRUM POTSDAM
GNSS	GLOBAL NAVIGATION SATELLITE SYSTEM
GNSS-RO	GLOBAL NAVIGATION SATELLITE SYSTEM – RADIO OCCULTATION
GPS	GLOBAL POSITIONING SYSTEM
GPS/MET	GLOBAL POSITIONING SYSTEM / METEOROLOGY
GRACE-FO	GRAVITY RECOVERY AND CLIMATE EXPERIMENT FOLLOW ON
GRACE	GRAVITY RECOVERY AND CLIMATE EXPERIMENT
IPCC	INTERGOVERNMENTAL PANEL ON CLIMATE CHANGE
KOMPASAT-5	KOREA'S MULTI-PURPOSE SATELLITE-5
LEO	LOW EARTH ORBIT
LRT	LAPSE-RATE TROPOPAUSE
METOP	METEOROLOGICAL OPERATIONAL SATELLITE
NASA	NATIONAL AERONAUTICS AND SPACE ADMINISTRATION
NOAA	NATIONAL OCEANIC AND ATMOSPHERIC ADMINISTRATION
NSPO	NATIONAL SPACE ORGANIZATION OF TAIWAN
PC	PRINCIPAL COMPONENT
PCA	PRINCIPAL COMPONENT ANALYSIS
QBO	QUASI-BIENNIAL OSCILLATION

RCP	REPRESENTATIVE CONCENTRATION PATHWAYS
RO	RADIO OCCULTATION
AS	SOUTH AMERICA
SAC-C	SATELLITE OF SCIENTIC APPLICATIONS-C
SH	SOUTH HEMISPHERE
SST	SEA SURFACE TEMPERATURE
TNA	TROPICAL NORTHERN ATLANTIC
TSA	TROPICAL SOUTHERN ATLANTIC
UCAR	UNIVERSITY CORPORATION FOR ATMOSPHERIC RESEARCH
UTC	UNIVERSAL TIME COORDINATED
USA	UNITED STATES OF AMERICA
WMO	WORLD METEOROLOGICAL ORGANIZATION

LIST OF SYMBOLS

°	Degrees
%	Percentage
Σ	Standard deviation
A	Bending angle
~	Approximately
A	Impact parameter
C	Celsius
e.g.	For example
eq.	Equation
F	Frequency
g/m^3	Gram per cubic meter
HPa	Hectopascal
Hrs	Hours
H_z	Hertz
i.e.	That is
K	Kelvin
K/dec	Kelvin per decade
K/km	Kelvin per kilometers
K/year	Kelvin per year
Km	Kilometers
Km/year	Kilometers per year
M	Meters
m/bar	Millibars
m/dec	Meters per decade
N	Refractive index
N	Refractivity
n_e	Electron density
P	Pressure
P_w	Pressure of the water vapor
r_t	Tangent point
S	Space

T	Temperature
t	Time
V_G	Speeds GNSS
V_L	Speeds LEO
W	Liquid water

CONTENTS

1 INTRODUCTION

South America (SA) may be considered a subcontinent of Americas, is located mostly in southern hemisphere, with a small portion in the northern hemisphere, with around 17,840,000 square kilometers. It has been facing the challenge of increasing food production and bioenergy, furthermore, the necessity to sustaining environmental quality in a climate change scenario, as observed by global temperatures rising and precipitation patterns changes. In southeastern South America, considering the period 1956-2003 the highest and lowest minimum temperatures increase significantly at a rate of 0.342°C and 0.542°C every 10 years, respectively (RUSTICUCCI & TENCER, 2008). In the Amazon region, two large droughts and three floods affected the region from 2005 to 2012 see e.g., (MARENGO et al., 2008, 2011, 2012, 2013; ESPINOZA et al., 2009, 2012, 2013; LEWIS et al., 2011; SATYAMURTY et al.,2013). The Andes temperature showed a significant warming trend of 0.28°C from 1979 to 2006. Throughout the Andean subtropical region in Argentina, the average annual temperature increased by 0.62°C during the 20th century, accompanied by a reduction of glaciers since the 1970s (MARENGO et al., 2011b). The Intergovernmental Panel on Climate Change (IPCC 2014) considering the Representative Concentration Pathways (RCP8.5) scenario showed temperatures projections indicating 4°C warming with around 15% rainfall reduction for the end of 21th century in SA.

Economic development in recent years, due to agricultural and industrialization frontiers expansion, consequently rises the potential for greenhouse gas emissions. Despite economic development, still exist in the majority countries of SA a high level of poverty. The vulnerability to floods, landslides, coastal erosion and lack of food due to agricultural droughts for the population living in such areas is considered high (e.g., floods in cities such as São Paulo and Buenos Aires) highlighting the importance to monitor temperature and understand its magnitude (MAGRIN et al., 2014).

Temperature variations in the troposphere and stratosphere are aggravated by greenhouse gases concentration. The tropopause is the transition zone in the atmosphere between the upper troposphere and the lower stratosphere, acting on the thermal equilibrium in this region. The tropopause temperature is sensitive to

temperatures variations in the troposphere and stratosphere. Similarly, the height of the tropopause tends to increase proportionally by the temperature variations occurring in the troposphere and stratosphere. Therefore, the mean height and temperature of the tropopause can act as climate change indicators (MELBOURNE et al., 1994; SANTER et al., 2003; SCHMIDT et al., 2008). The mean global tropopause height presents an upward trend in the reanalysis and radiosonde observations for the period from 1979 to 2001 (SANTER et al., 2004). However, the limitations of vertical resolution in the reanalysis, radiosonde models and few radiosonde data distributed homogeneously on the globe are still obstacles to accurately identifying the tropopause.

The atmospheric remote sensing technique known as GNSS Radio Occultation (GNSS-RO) makes use of GNSS (Global Navigation Satellite System) signals in conjunction with Low Earth Orbit (LEO) satellites, e.g. CHAMP (Challenging Minisatellite Payload), GRACE (Gravity Recovery and Climate Experiment) and FORMOSAT-3/COSMIC (Constellation Observing System for Meteorology Ionosphere & Climate). The main problems related to radiosondes and reanalysis models are the low vertical resolution and inhomogeneous distribution of data on the globe. GNSS-RO overcomes these limitations due to the precision of the GNSS technique. The GNSS-RO observations have higher vertical profile resolution (~ 0.5 to 1.5km), data distributed almost evenly across the globe, including the oceans. The GNSS-RO technique does not require active calibration and maintains the long-term system stability excluding problems such as time series discontinuities (MELBOURNE et al., 1994). Global studies of tropopause showing trends derived from GNSS-RO, see e.g., Schmidt et al. (2008) and regional studies, see e.g. Khandu et al. (2011); Khandu, Awange & Forootan, (2016), pointed to increasing height and decreasing temperature in tropopause.

1.1 OBJECTIVES

In this section we present the general and specific objectives of this dissertation.

1.1.1 General objective

The general objective of this research is to investigate the tropopause height and temperature considering South America between 2001 and 2017 (17 years), using GNSS-RO data from CHAMP, GRACE and COSMIC.

1.1.2 Specific objectives

- Validate GNSS-RO with atmospheric observations of temperature obtained from radiosonde in South America.
- Compare the tropopause height and temperature trends found in South America with global tropopause tendencies e.g. (SEIDEL & RANDEL, 2006; SCHMIDT et al., 2008).
- Correlate the tropopause height and temperature variability with the teleconnections.

1.2 DISSERTATION STRUCTURE

The second chapter describes the radiosonde as a classical method for obtaining atmospheric profiles, presents the theoretical basis of the GNSS-RO technology and the atmospheric oceanic indexes representing the teleconnections. The chapter 3 presents the study area (South America), radiosonde data and GNSS-RO, describing the methodology applied for the validation of the GNSS-RO data and obtaining the height and temperature of the tropopause. In chapter 4 are the results, including the validation of the data, analysis of the trends of the height and temperature of the tropopause and correlation between the variability of the tropopause in South America with the teleconnections. Chapter 5 finalize with conclusions and recommendations.

2 THEORETICAL FOUNDATION

Radiosonde is the classic method for obtaining atmospheric profiles. In the sequence it is presented the obtaining radiosonde data, the theoretical concept of the GNSS-RO technology with a summary of the space missions and the occultation geometry, the grounding of the teleconnections and the indexes used in this dissertation.

2.1 RADIOSONDE

The radiosondes, altitude meteorological stations, are equipped with sensors of temperature, humidity, pressure and a GNSS receiver responsible for determining the sounding altitude. By traversing the tropospheric vertical profile using a balloon inflated with hydrogen or helium, the radiosonde collects dynamic and thermodynamic variables of the atmosphere (e.g., pressure, temperature, humidity, wind speed and direction) at various levels of altitude in the atmosphere, as it the passes through the layers of the atmosphere, the radiosonde sends the data, via radio to the ground station (Fig.1). The radiosondes provide data between the surface of the Earth and approximately 30 km of altitude with average vertical resolution of about 50 m, in good weather conditions, altitudes of up to 40 km can be reached (WICKERT, 2004b). Atmospheric profiles obtained by radiosonde have been recorded since the 1970s, providing a significant time series for several studies, being an extremely important tool to support climate monitoring and forecasting.

Figure 1 - Scheme of the launching and transmission of radiosonde data.

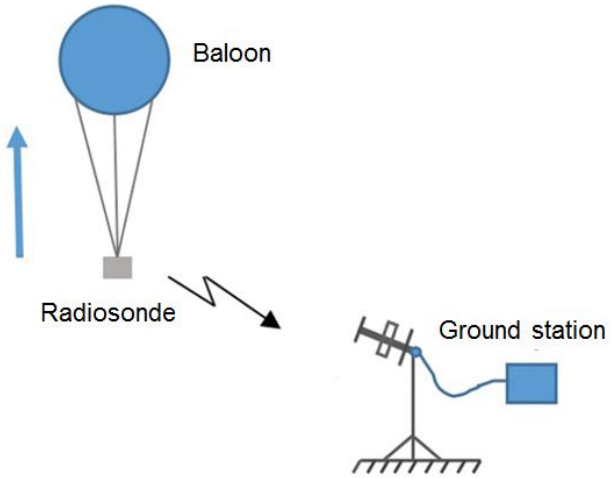

Source: Adapted from OLIVEIRA, AMORIM & DERECZYNSKI (2018)

2.2 GNSS-METEOROLOGY/RADIO OCCULTATION (RO)

On April 1995, the US launched the Microlab-1 satellite considered LEO (Low Earth Orbit) to investigate the GNSS-RO potential in obtaining neutral atmosphere and ionosphere data, the mission became known as GPS/MET (Global Positioning System/Meteorology) and collected atmospheric data from 1995 to 1997. The GPS/MET receiver built by NASA (National Aeronautics and Space Administration) is a GPS receiver that produces only a small number of RO probes (~ 125) per day, many of the probes have failed in the lower troposphere (3 to 5km above the surface). However, GPS/MET provided a huge insight about the GNSS-RO signals behavior, which led to a new design for the next-generation occultation receivers (JIN, CARDELLACH & XIE, 2014).

After the success of the mission, several countries carried out their own scientific missions. The CHAMP (Challenger Minisatellite Payload) mission launched in a near-circular orbit with an initial elevation of 454 km and an inclination of 87.2° on July 15, 2000, by Germany in partnership with USA for magnetometry and gravity mapping also providing GNSS-RO data between 2001 and 2008. The CHAMP uses the GPS radio occultation technique to provide globally distributed atmospheric profiles, the vertical resolution ranges from 0.5km in the troposphere to less than 1.5km in the stratosphere (WICKERT et al., 2001, 2005, 2009; TAPLEY et al., 2004).

The GRACE (Gravity Recovery and Climate Experiment) mission is a partnership between the agencies, NASA and DLR (Deutsche Forschungsanstalt für Luft und Raumfahrt), consisting of two satellites separated by 220km orbiting the Earth from March 17, 2002 at an initial altitude 500km and an almost circular orbit of 89.0° inclination. The GRACE mission is designed to track changes in Earth's gravitational field for a period of five years, the mission was in operation until December 2017, in 2018 GRACE-FO (Gravity Recovery and Climate Experiment Follow On) was launched, which continues the GRACE mission (TAPLEY et al., 2004; WICKERT et al., 2005, 2009).

The FORMOSAT-3/COSMIC (Constellation Observing System for Meteorology Ionosphere & Climate) is a partnership between the University Corporation of Atmospheric Research (UCAR), and the National Space Organization of Taiwan (NSPO). This is a scientific mission to develop observation techniques using GNSS signals for weather forecasting and climate analysis. On April 14, 2006 the Formosat-3/COSMIC mission entered orbit with a constellation of six LEO satellites with low-inclination (equatorial) orbits with 516km altitude, generating 2,500 probes per day, distributed globally, with data available from 22 April 2006 (FONG et al., 2008; JIN, CARDELLACH & XIE, 2014).

The European Union Meteorological Operational Satellite (METOP), launched on 19 October 2006, is the first polar orbiting satellite in Europe to provide data for climate forecasting and monitoring. The SAC-C (Satellite of Scientific Applications-C) that carries a multispectral imager and a magnetometer launched in 2000 by Argentina-USA partnership. TERRASAR-X launched by Germany and in operation since 2008. The South Korean mission KOMPSAT-5 (Korea's Multi-Purpose Satellite-5) has been in operation since 2015. As well as a number of other missions with RO receivers are planned such as the Chinese FY-3C (Feng-Yun 3C); ROHP-PAZ of Spain and EQUARS (Equatorial Atmosphere Research Satellite) of Brazil (2020). The increase of the GNSS-RO constellation can have a profound impact on long-term climatological studies and short-term weather forecasts (JIN, CARDELLACH & XIE, 2014).

The GNSS radio occultation technique (RO) is based on accurate double-frequency measurements (L-band) made by a GNSS receiver on board of a LEO satellite that receives the signals transmitted by the GNSS satellite constellation. Radio occultation occurs when the GNSS satellite, which is opposite to the LEO

receiver satellite, transmits a signal tangent to the atmosphere, i.e. occult by the horizon (Fig.2), as the LEO satellite and GNSS move, the signal crosses the various layers of the atmosphere which leaves the path traveled by the slightly flexed signal. The other satellites of the GNSS constellation that are not in the geometric position to perform the radio occultation are used to accurately determine the positions, speeds and GPS and LEO clocks errors (JIN, CARDELLACH & XIE, 2014).

Figure 2 - Radio occultation geometry composed by: GNSS RO occult by the atmosphere, reference GNSS (not occult), GNSS LEO (receiver of the radio occultation) and ground station.

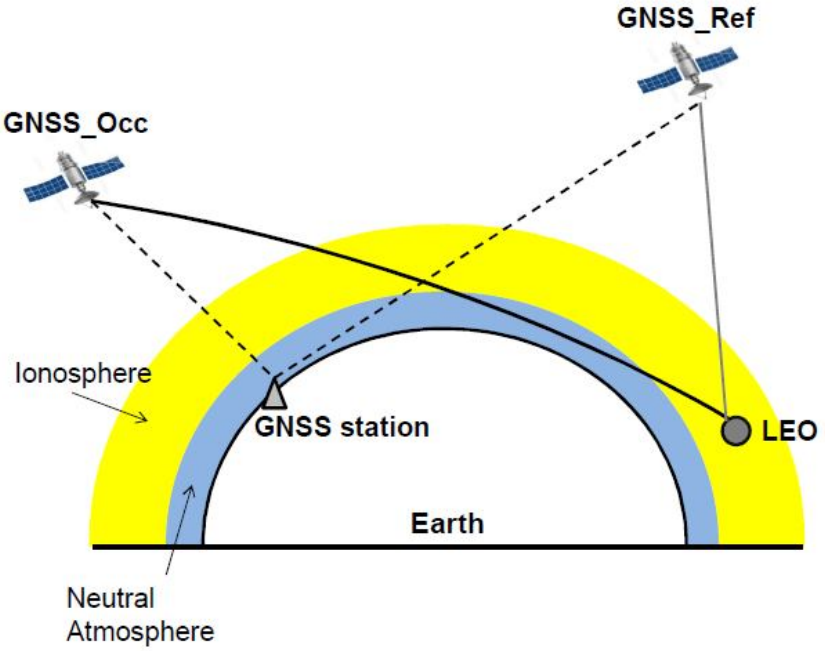

Source: Adapted from JIN, CARDELLACH & XIE (2014).

As the light pathways bend during an occultation event, the signal delay received by the LEO satellite is observed as a difference in signal phase and amplitude. The changes in the GPS signal when passing through the atmosphere are described by three parameters (Fig.3), the angle of bending (α), an impact parameter (a) and a tangent radius (r_t) (AWANGE & GRAFAREND, 2005).

Figure 3 - Geometry of an occultation, in which (α) is the signal curvature angle, (a) the impact parameter and (rt) the tangent point, both representing the signal variation parameter. The vectors VG and VL are the speeds of the GNSS and LEO satellites, respectively.

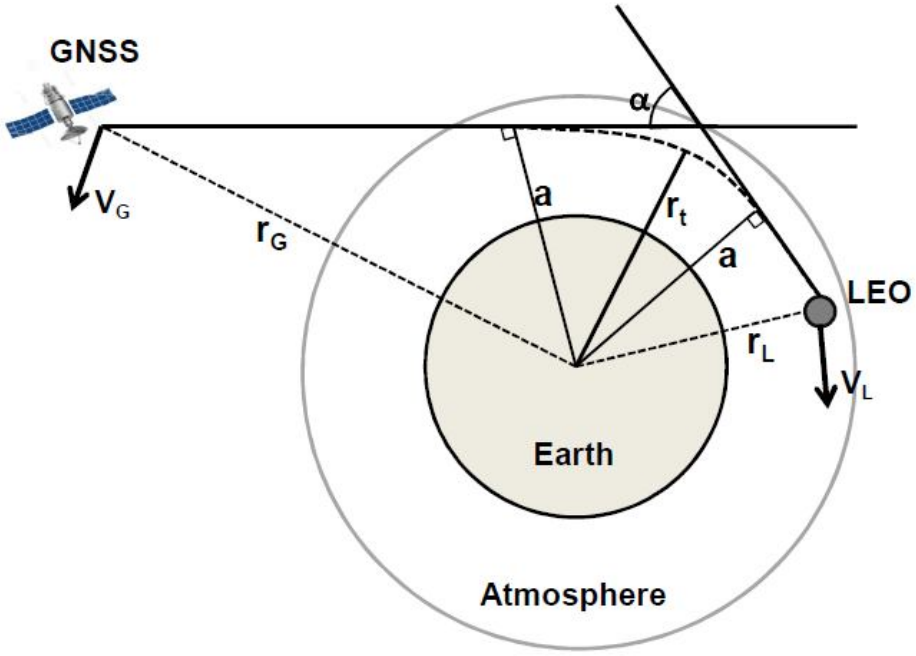

Source: Adapted from JIN, CARDELLACH & XIE (2014).

The relationship between the bending angle (α) caused by the atmospheric refraction, the impact parameter (*a*) (the radial distances for the beginning and signal bending ending) and the refractive index (*n*) is given by equation 1, (AWANGE & GRAFAREND, 2005):

$$\alpha(a) = 2a \int_{r=r_0}^{r=\infty} \frac{1}{\sqrt{n^2 r^2 - a^2}} \frac{d\ln(n)}{dr} dr \,. \qquad (1)$$

Using the Abel transformation to express the bending angle deduced from the position and velocity of the GNSS and LEO satellites as a function of the parameter *a* it is possible to obtain the refractive index, *n*, presented in equation 2 (AWANGE & GRAFAREND, 2005):

$$n(r_0) = exp\left[\int_{a=a_0}^{a=\infty} \frac{\alpha(a)}{\sqrt{a^2 - a_0^2}} da\right] \qquad (2)$$

Where, r_0 is the radius relative to the center of the Earth. From the refractivity *N*, which is related to the refractive index *n*, using empirically determined coefficients the atmospheric parameters, such as temperature, pressure and air density, are calculated in equation 3 (AWANGE & GRAFAREND, 2005)::

$$N = (n-1)10^6 = 77.6\frac{P}{T} + 3.73 \times 10^5 \frac{P_w}{T^2} - 40.3 \times 10^6 \frac{n_e}{f^2} + 1.4w, \quad (3)$$

Where *P* is the air pressure in *mbar*, *T* is the air temperature in *K*, P_w is the partial pressure of the water vapor in *mbar*, n_e is the electron density per cubic meter in number of *electrons/m*$^{-3}$, *f* is the frequency of the transmitter in H_z and *w* is the liquid water content in g/m³. In equation 3, the refractivity *N* receives three main contributors in the first term by dry neutral atmosphere (called dry component) in the second term the water vapor (also called wet components) and the third term are the free electrons in the ionosphere (AWANGE & GRAFAREND, 2005).

2.3 TELECONNECTIONS

The teleconnections are important parameters to explain the regional anomalies occurrence associate with remote regions anomalies. The term “teleconnection” refers to a recurrent and persistent anomalies pattern of a particular variable, which may persist for several weeks, months, or years, thus showing an important part of the interannual and interdecadal climate variability of the atmosphere (CAVALCANTI & AMBRIZZI, 2009). In this study, teleconnections are represented by three ocean-atmospheric indexes: (i) quasi-biennial oscillation (QBO), (ii) El Niño and the Southern Oscillation (ENSO), and (c) SST-Atlantic, which are commonly associated with significant fluctuations in the temperatures of the upper troposphere and lower stratosphere.

The Quasi-Biennial Oscillation (QBO) is characterized by east-west descending wind regimes, with a variable period of approximately 28 months. The QBO dominates the variability of the equatorial stratosphere, although it is a tropical phenomenon, it affects the stratospheric flow from pole to pole with extratropical dynamic effects in the troposphere and mesosphere. By modulating the propagation of extratropical waves the QBO has an effect on the breaking of the stratospheric polar vortices that affect the surface weather patterns, providing the mechanism for

QBO to have an effect on the Earth surface (BALDWIN et al., 2001). Angell & Korshover (1964), showed the evidence of almost biennial oscillations in stratospheric temperature and tropopause, with a good correspondence between the QBO variation's in height of the tropopause in relation to the QBO variation of the temperature in the lower stratosphere. Reid & Gage (1985), found that the tropopause height has a significant QBO dependence in the tropical stratosphere and the temperature anomalies El Niño-Southern Oscillation (ENSO).

ENSO is the phenomenon characterized by Sea Surface Temperature (SST) anomalies in the Pacific Ocean. The hot and cold phases of the ENSO are called El Niño and La Niña events, during periods under El Niño influence, there is a positive anomaly of SST values along the Peru coast and negative values near the Australia coast. The phenomenon La Niña is characterized by the opposite situation.

The ENSO event can occur when SST anomalies exceed 0.4°C for 6 months or more (TRENBERTH, 1997). To characterize ENSO events, two oceanic indexes (Fig.4) are used: (i) Niño 3.4 (5°N - 5°S, 120°W - 170°W) index that corresponds to the equatorial anomalies of the SST to the east of the coast line of South America, (ii) Niño 1+2 (0° - 10°S, 90°W - 80°W) corresponding to the region with the smallest area of extension and the largest variance of the Niño SSTs regions (TRENBERTH & STEPANIAK, 2001), fitting in this study, considering the eastern region and SA west coast correspondence. Several studies have found that together with the ENSO, the SST - Atlantic has influenced the precipitation regime variability over SA, see e.g., Moura & Shukla (1981); Andreoli et al., (2004); Giannini, Saravanan & Chang, (2004); Santos & Brito (2007). For the teleconnection with the Atlantic Ocean (Fig.4), two indices are also used: (i) Tropical Southern Atlantic (TSA) using the range between 0° and 20°S and between 30°W and 10°E, (ii) Tropical Northern Atlantic, (TNA) where the anomalies of SST are calculated between 5.5°N and 23.5°N and between 57.5°W and 15°W. The QBO, Niño 3.4, Niño 1+2, TSA and TNA indices are obtained from the National Oceanic and Atmospheric Administration (NOAA).

Figure 4 - Regions of the ENSO indexes (Niño 3.4 and Niño 1 + 2) and SST - Atlantic (TSA and TNA).

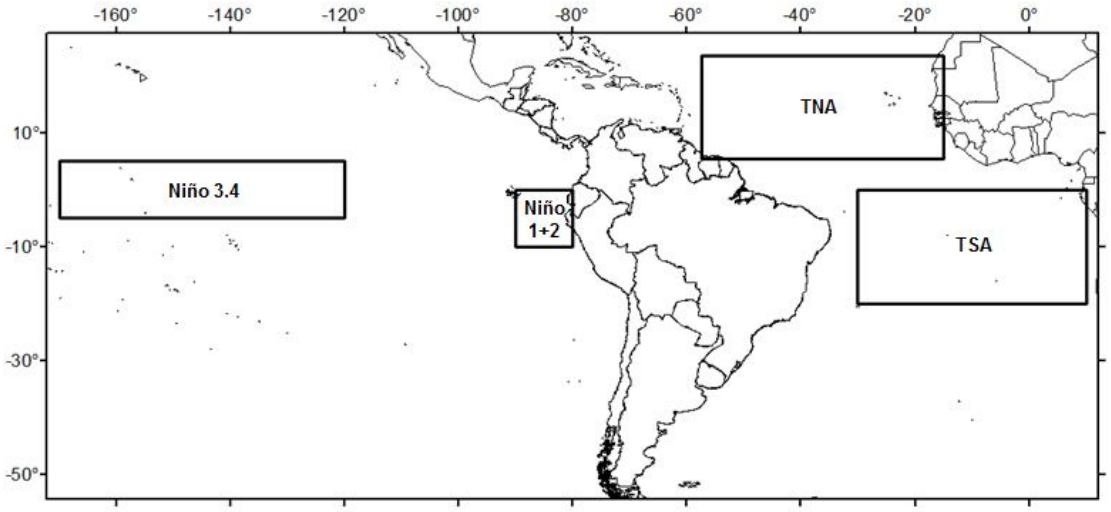

Source: The Author (2018).

To study the temperature and height variations of the tropopause in relation to the teleconnections the PCA (Principal Component Analysis) is applied to the anomalies of height and temperature of the tropopause. The PCA is an exploratory statistical data tool used in atmospheric/oceanic science because it allows a spatial and temporal decomposition of geophysical data (e.g. temperature) according to the main factors of variability in the atmosphere (RANDEL, WU, & GAFFEN, 2000; GETTELMAN et al., 2001; KHANDU, AWANGE & FOROOTAN, 2016). The PCA applied to the tropopause anomalies finds a set of spatial patterns called Empirical Orthogonal Functions (EOFs), together with a set of uncorrelated temporal series or Principal Components (PCs) that is obtained by the projection of each EOF in the original data of anomaly (eq. 4), the PCA results explain most of the observed variance (expressed as a percentage) of spatial-temporal data (PREISENDORFER, 1988; KHANDU, AWANGE & FOROOTAN, 2016).

$$P_{(t,n)} = X_{(t,s)} E_{(s,n)}, \qquad (4)$$

To apply PCA, the series must be in matrix format, in eq. 4, $X_{(t,s)}$ is the matrix of the data, where t is the temporal component and is the spatial component of the height and temperature anomalies, $E_{(s,n)}$ is a matrix of orthogonal functions, where n is a number of functions and the matrix $P_{(t,n)}$ are the main components of the variability distributed throughout the time series.

3 MATERIALS AND METHODS

This section describes South America as a study area, presents the format and acquisition of the radiosonde and GNSS-RO data, describing the methodology applied for the validation of the GNSS-RO data and obtaining the height and temperature of the tropopause. The processing steps were performed by Matlab software.

3.1 STUDY AREA

South America (SA) has a large latitudinal range, from equatorial areas to medium latitudes. The relief varies between the Andes Mountain Range and several plateaus and plains. The Amazon rainforest in northern SA has dense vegetation cover and high seasonal rainfall zone. These conditions vary to the extreme opposite, considering the Atacama Desert. All combined factors contribute to different types of climatic regimes in this region, making SA an excellent opportunity to study trends in tropopause heights and temperatures. The boundary of the study area is between 20°N and 60°S (latitudes) and 90°W at 30°W (longitudes), involving the continental area and part of the adjacent oceans, bordering Pacific in the west and Atlantic in the east.

Figure 5 shows the study case limits and radio occultation observations locations considering 2007 (Fig. 5a) and 2008 (Fig. 5b), for four observation sources: COSMIC (green dots), CHAMP (red dots), GRACE (blue dots) and radiosonde (black triangles) stations. Fig. 4a shows 4,706 occultation provided by CHAMP, 2,443 by GRACE and 69,867 by COSMIC. Fig. 5b shows 3,597 occultation for CHAMP with is smaller in relation to 2007 because the mission provided data until October of 2008, it also shows 3,147 by GRACE and 69,756 by COSMIC.

Figure 5 - Radio occultation observations for the years (a) 2007 and (b) 2008 as measured by COSMIC (green points), CHAMP (red points) and GRACE (blue points) satellites. The black triangles indicate the 54 radiosonde stations.

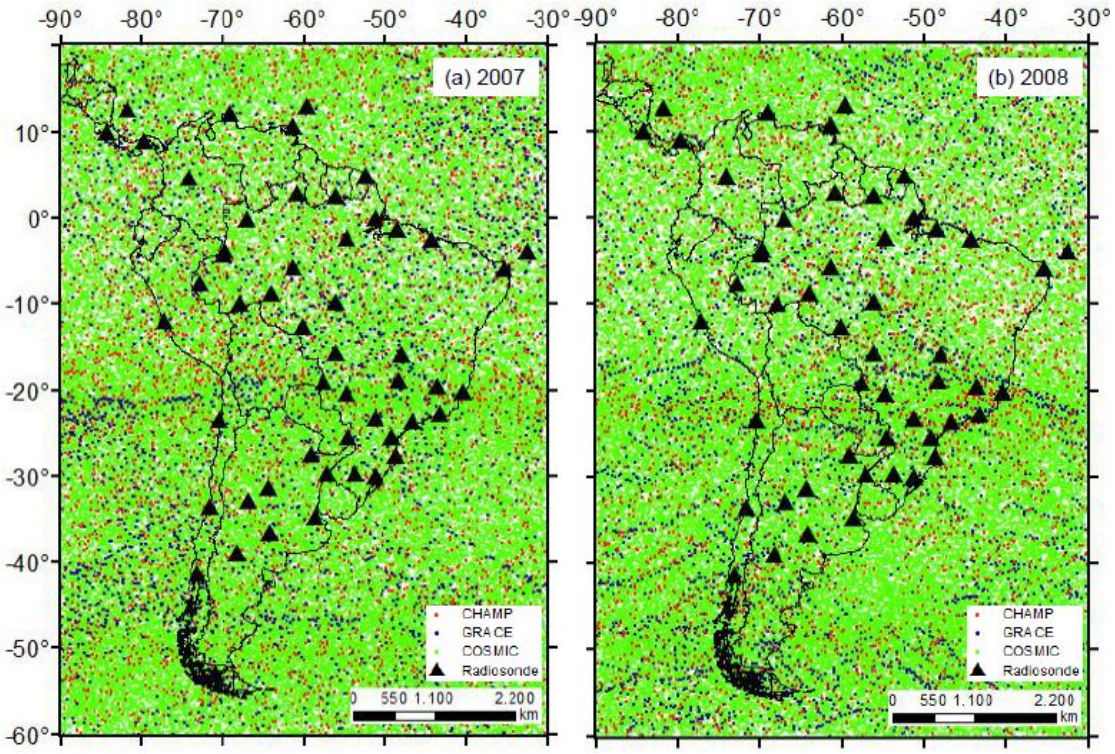

Source: The Author (2018).

3.2 DATA

Radiosonde data were provided by The Department of Atmospheric Sciences, University of Wyoming. Most stations are located at the major airports in South America (Fig. 5), the radiosonde observations are collected daily, every 12 hours and provided atmospheric parameters (such as temperature and pressure profiles) at standard pressure levels (e.g. 850hPa, 700hPa, etc.). The radiosondes atmospheric profiles are used for validation criteria considering the GNSS-RO data set from CHAMP, GRACE and COSMIC. Table 1 summarizes the main differences between the radiosonde and GNSS-RO data. Radiosondes have punctual spatial distribution mainly located at airports whereas the GNSS-RO data provides occultation according to the GNSS satellite orbit which allows points distributed almost everywhere around the Earth including over the oceans. Considering the temporal distribution, each radiosonde collects 2 atmospheric profiles per day (every 12hrs, in general at 00:00

and 12:00 UTC). The GNSS-RO for the same reason mentioned above collects a greater number of occultation per day at different times.

Table 1 - Data source, provider, and spatial and temporal distribution.

Data	Provider	Source	Spatial Distribution	Temporal Distribution
Radiosonde	University of Wyoming		Fixed points(e.g. Airports)	Every 12 hrs (e.g. 0h/12h)
CHAMP-RO	CDAAC	NASA/GFZ	Homogeneous	Homogeneous
GRACE-RO	CDAAC	NASA/GFZ	Homogeneous	Homogeneous
COSMIC-RO	CDAAC	UCAR/NSPO	Homogeneous	Homogeneous

Source: The Author (2018).

The GNSS-RO data from CHAMP, GRACE and COSMIC missions were provided by the UCAR (University Cooperation for Atmospheric Research) CDAAC (COSMIC Data Analysis and Archive Center) processing center. The level 2 data format, available in CDAAC, contains refractivity profiles inverted by Abel transformation with air temperature, water vapor, air pressure, height above mean sea level and location of radio occultation (KHANDU et al., 2011). In this study were selected the variables: altitude, pressure, temperature and hiding position.

The CHAMP satellite provided 33,824 atmospheric profiles uniformly distributed in the study area during the period from May 19, 2001 to October 5, 2008 (Fig. 6a). The CDAAC provides GRACE data from February 28, 2007 to July 31, 2017, a total of 38,764 GRACE radio occultation as shown in Fig. 6c. The COSMIC radio occultation data for the period from April 22, 2006 to December 31, 2017 registered 550,326 atmospheric profiles distributed in the study area according with Fig. 6b. The Fig. 6d shows the annual distribution of the data considering these missions and highlights that since 2006 the COSMIC mission contributes with a greater amount of data compared with the CHAMP and GRACE.

Figure 6 – Monthly distribution of GNSS-RO data for South America. (a) CHAMP from 2001 to 2008, (b) COSMIC 2006 to 2007, (c) GRACE 2007 to 2017, and (d) annual distribution of the three data series.

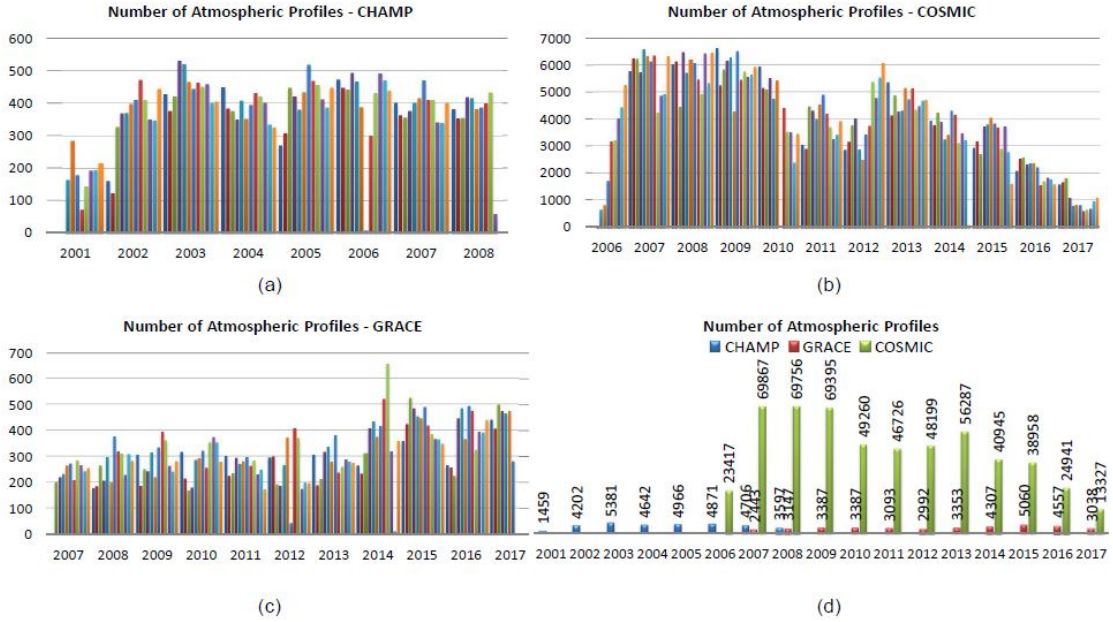

Source: The Author (2018).

3.3 METHODOLOGY

Figure 7 shows the methodological flowchart used in this dissertation. In the following the atmospheric profiles obtained by radiosondes will be used as reference for validation of atmospheric profiles of GNSS-RO data based on statistical criteria established in Wickert, (2004b). If the validation is accepted, the height and temperature of the tropopause of each atmospheric GNSS-RO profile will be extracted, otherwise the GNSS-RO sample will be discarded. Using the time series of the validated GNSS-RO data will be calculated the trend of the height and temperature of the tropopause to South America. The last step is to verify, through the PCA, if there is correlation in the variability of the height and temperature of the tropopause with teleconnections.

Figure 7 - Shows flowchart the methodology used to validate the height and temperature profiles of the tropopause.

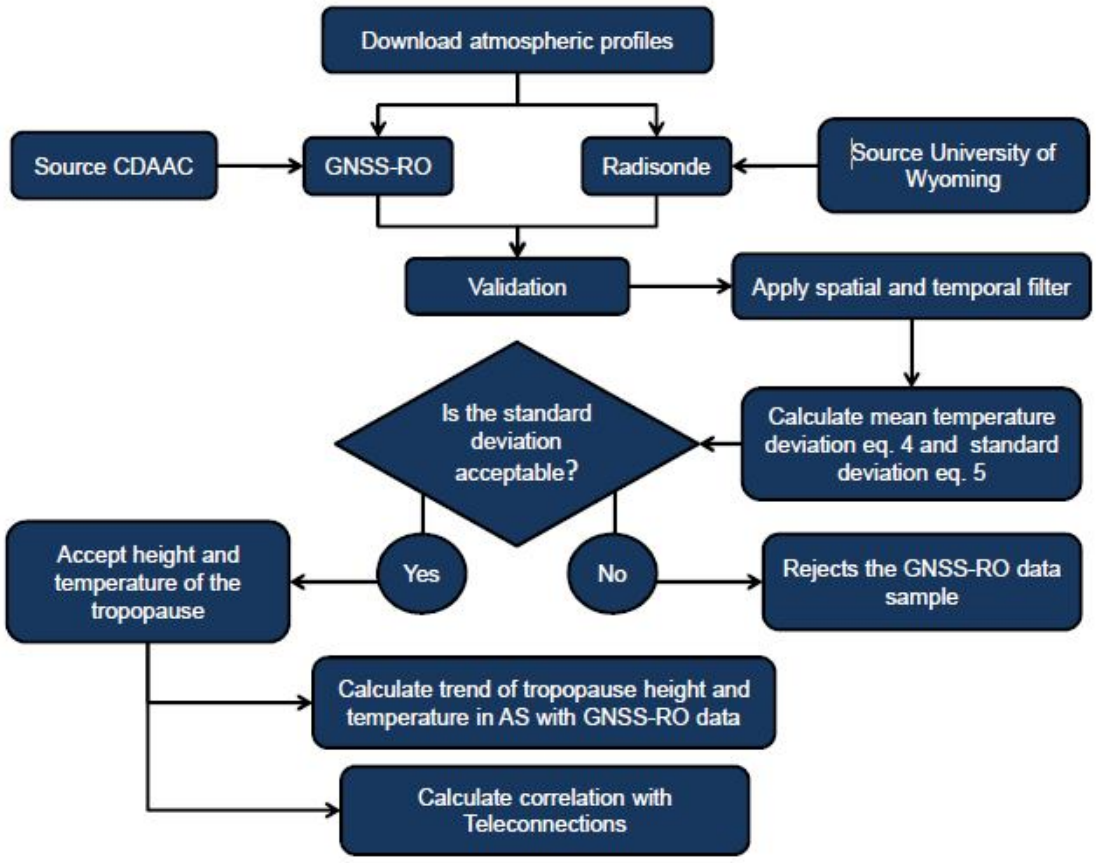

Source: The Author (2018).

3.3.1 GNSS-RO temperature profiles validation

The GNSS-RO temperature profiles are compared to radiosonde observations at 17 standard pressure levels between 850hPa and 20hPa. As the spatial and temporal distribution of the radiosonde and GNSS-RO data are different, to ensure that the GNSS-RO atmospheric profiles to be compared with the radiosondes are in the same climatic conditions it is necessary to select: (i) GNSS-RO profiles that are spatially separated by a radius less than 100 km radiosonde; (ii) the difference between the screening time of the GNSS-RO profile and that of the radiosonde is less than 3 hours (WICKERT, (2004b). With selected profiles it is calculated the mean temperature deviation $\Delta T(l)$ at each pressure level and its corresponding

standard deviation $\sigma_{\Delta T}(l)$ are obtained using equations 5 and 6 respectively, (WICKERT, (2004b):

$$\overline{\Delta T(l)} = \sum_{i=1}^{M(l)} T_{D(GNSS-RO)}(i,l) - T_{RS}(i,l) , \quad (5)$$

and

$$\sigma_{\Delta T}(l) = \sqrt{\frac{1}{M(l)-1}\sum_{i=1}^{M(l)}(T_{D(GNSS-RO)}(i,l) - T_{RS}(i,l))^2} , \quad (6)$$

Where $M(l)$ denotes the number of data points per pressure level, i is the individual RO and radiosonde data, $T_{D(GNSS-RO}$ is the temperature derived from the satellite data, and T_{RS} is the temperature given by the radiosonde measurements. In this analysis, any temperature deviations obtained using (eq. 5) that were greater than 20K were discarded to reduce outliers influence (WICKERT, (2004b).

Wickert, (2004b) e.g. compared the compare the temperature profiles obtained by CHAMP with radiosonde observations in different geographic regions (Australia, China, Europe, India, Japan, countries of the former SU and USA and the results between CHAMP and radiosonde showed a bias less than 1K and standard deviation less than 2.7K. Holzschuh, Sapucci & Monico, (2010) compared the atmospheric profiles obtained with the CHAMP satellite over South America with radiosonde profiles, the result indicated a bias below 1K and a standard deviation of up to 3K in the atmospheric layer between 9 and 18 km in the atmosphere.

3.3.2 Tropopause heights and temperatures derivation

This dissertation focuses on interannual variations in the first tropopause known as LRT (Lapse-Rate Tropopause) that is defined by the WMO (World Meteorological Organization - 1957) as the lowest level where the lapse rate decreases 2K/km or less, provided that the average lapse rate between that level and all other higher levels within 2km does not exceed 2K/km, (WMO, 1957). The tropopause height and temperature obtained in the atmospheric profiles GNSS-RO are based on the definition provided by the WMO-1957.

As the height of the tropopause is strongly dependent on latitude, the study area (20°N - 60°S) was divided into three different zones (see Table 2). The GNSS-

RO dataset mean and standard deviation associated with each zone are calculated monthly. The differences between monthly averages and annual averages produce a monthly time series of tropopause anomalies (height and temperature). The linear trends are based on height and temperature anomalies calculated from the annual averages. To avoid outliers, monthly data with more than three times the standard deviation, under this criterion for each zone are discarded (KHANDU et al., 2011).

Table 2 - The South America subdivisions considering latitudinal zones to analyze height and temperature.

Zone	Latitudes
Tropics	20°N - 20°S
Subtropics	20°S - 40°S
Mid-latitudes	40°S - 60°S

Source: The Author (2018).

4 RESULTS AND DISCUSSIONS

Results include validation of GNSS-RO data, latitudinal and seasonal analysis of tropopause, trends in tropopause height and temperature, and correlation between tropopause variability in South America and teleconnections through PCA**.**

4.1 RO TEMPERATURE PROFILES VALIDATION

Before determining the tropopause height and temperature, it is necessary to ensure that the GNSS-RO atmospheric profiles are compatible with the radiosonde data and therefore whether they are suitable for climatic variability studies.

Figure 8 shows a comparison between the atmospheric temperature profiles obtained from radiosondes with GNSS-RO profiles of CHAMP missions (Fig. 8a, 8d), GRACE (Fig. 8b, 8e) and COSMIC (Fig. 8c, 8f). Radiosonde stations were distributed spatially at six airports to cover latitude and longitude variations in South America. The dates of the atmospheric profiles were randomly selected between 2001 and 2017. The temperature atmospheric profiles obtained by CHAMP are compared with the radiosondes at Corozal airports (Fig. 8a) on September 27, 2004 (lat: 8.9°, long: -79.6°) and Santo Domingo (Fig. 8d) at n November 3, 2007 (lat: -33.6°, long: -71.6°). For the GRACE profiles, the radiosonde observations of the Alta Floresta airport (Fig. 8b) were used on July 16, 2008 (lat: -9.9°, long: -56.1°) and at the airport of Foz do Iguaçu (Fig. 8e) on August 17, 2014 (lat: -25.5°, long: -54.6°). COSMIC profiles are compared to radiosondes at Belém airport (Fig. 8c) on July 18, 2007 (lat: -1.3°, long: -48.5°) and Vitória airport (Fig. 8f) on September 23, 2014 (lat: -20.3°, long: -40.3°). In all comparisons, GNSS-RO profiles were selected that were closer to the radiosonde stations, according to the criteria (i) and (ii) established in section Sec .3.3.1 that are been separated spatially by a radius less than 100km and with a time interval shorter than 3 hours in relation to the radiosonde profile (WICKERT, 2004b).

Figure 8 - Compares the radiosonde profiles obtained at six airports with the atmospheric profiles obtained from CHAMP, GRACE and COSMIC for the period from 2001 to 2017 which matches with radiosondes observations between 8km and 25km.

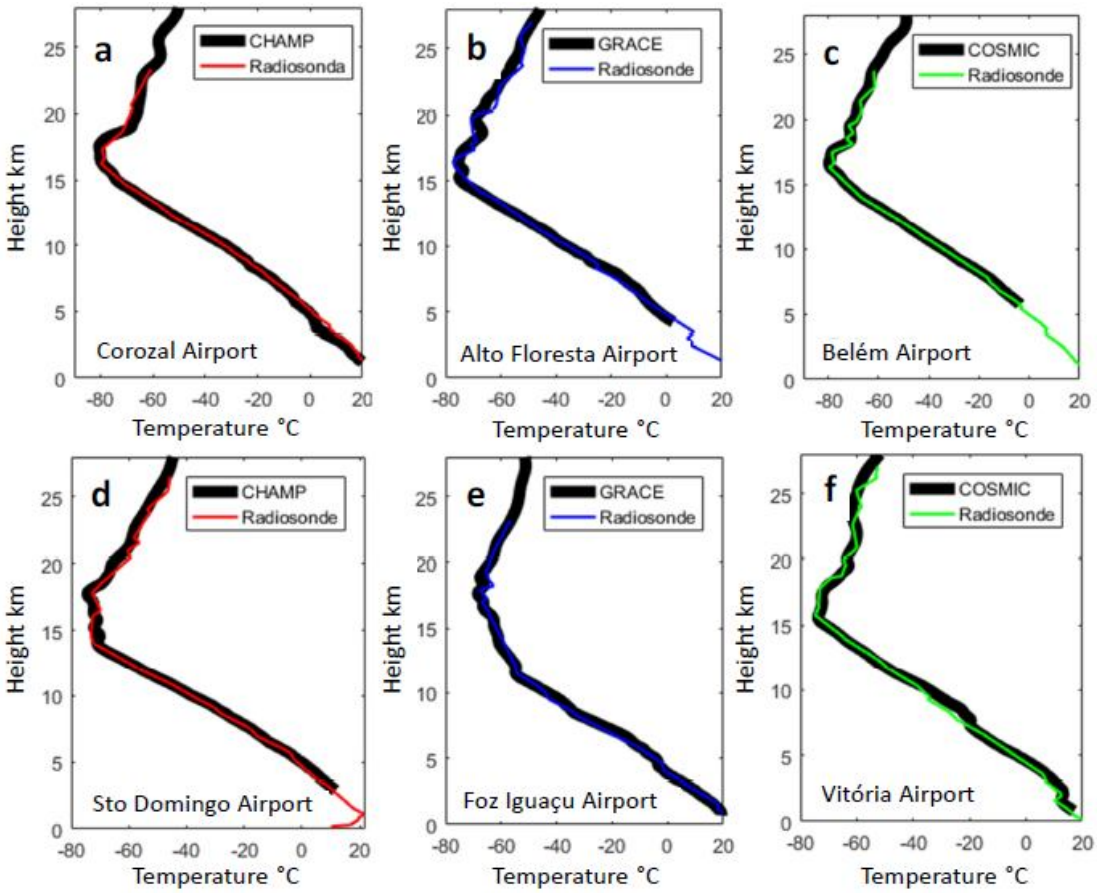

Source: The Author (2018).

Analyzing Fig. 8, COSMIC temperature profile showed the best fitting with the corresponding radiosonde profile with a near zero bias between 10km and 24km. CHAMP, GRACE and COSMIC profiles matches with the observations of the radiosonde between 8km and 25km, with small heights deviations above 16km. Considering the water vapor presence, the profiles obtained by the 3 missions showed a larger bias in relation to radiosonde, similar with the results presented by Wickert et al., (2005) considering CHAMP profiles.

Figure 9 shows the GNSS-RO validation results of temperature profiles at 17 pressure levels, the mean temperature deviation ΔT (eq. 5) and its corresponding standard deviation $\sigma_{\Delta T}$ (eq. 6) for all the GNSS-RO profiles (CHAMP, GRACE and

COSMIC) compared with 54 radiosonde stations in South America during the period from 2001 to 2017, selected considering the criteria in Sec.3.3.1.

Figure 9 - Comparison between GNSS-RO temperature and radiosonde observations for South America between 2001 and 2017, presented as mean and standard deviation. (a) Comparison of CHAMP and radiosonde temperature estimates from May 2001 to October December 2008. (b) GRACE RO profiles from February 2007 to July 2017. (c) COSMIC profiles from April 2006 to December 2017. (d) Number of GNSS-RO profiles used.

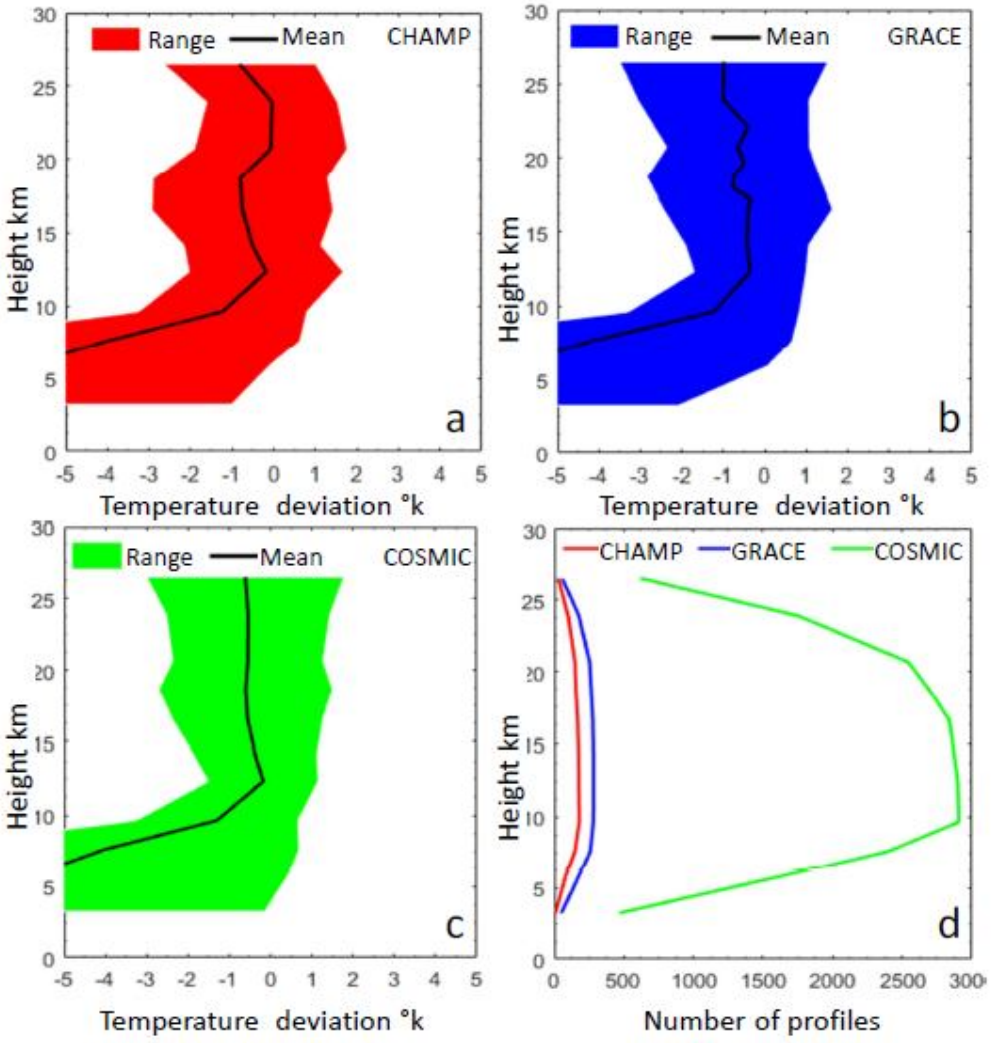

Source: The Author (2018).

The CHAMP dataset between May 2001 and October 2008 with 168 profiles (Fig. 9d) were used for the comparison with the radiosonde observations and showed a bias below 1K for heights between 10km and 26.5km, with a maximum standard

deviation of 2.1K (Fig. 9a). For GRACE data, 460 profiles were selected (Fig. 9d) from February 2007 to July 2017. The deviation between 10 and 26.5km is less than 1K with a maximum standard deviation of 2.1K (Fig. 9b). The COSMIC data, from April 2006 to December 2017 provided 2,915 (Fig. 9d). The results indicate temperature deviations less than 0.6K ranging between 10km to 25km, with standard deviations less than 2K (Fig. 9c).

It is possible to notice that below 9km the temperature standard deviation suffers a significant increase of the negative bias that is associated with the presence of water vapor. Below that altitude the GNSS-RO temperature estimates are significantly affected by water vapor, which is neglected during the Abel transformation (MELBOURNE et al., 1994; WICKERT et al., 2004; AWANGE & GRAFAREND, 2005; ANTHES et al., 2008).

Comparing the three missions' profiles, it is possible to observe a bias less than 1K between 10km and 25km among GNSS-RO temperatures and radiosonde. The COSMIC dataset presented the best results compared with the others, besides providing significantly more profiles (Fig. 6d) also presented better results for the average temperature, showing results below 0.6K and less deviations between 10 and 18km with less than 2.1K.

4.2 TROPOPAUSE HEIGHTS AND TEMPERATURES

Figure 10 shows the tropopause (height and temperature) monthly average in SA between May 2001 and December 2017, according to RO data from CHAMP, GRACE and COSMIC. The mean tropopause height and temperature are calculated monthly and have a cyclic pattern. In summer (January - March), the height highest values are accompanied by the lower temperatures, while in the winter (July - September) this cycle is inverted, presenting the tropopause lowest heights and higher temperatures. The monthly tropopause average for South America between 2001 and 2017 is 14.18 ± 0.52km for height with average temperature of 203.46 ± 1.55K. The monthly height average peaks are July 2006 with 12.92Km and January 2005 with 15.62km (Fig. 10b), these months also corresponding to the peaks for monthly temperature average (Fig. 10a), being July 2006 with 206.98K, and January 2005 with 198.88K.

Figure 10 - Monthly tropopause mean (a) temperature and (b) height for South America using the GNSS-RO data for the period between 2001 and 2017.

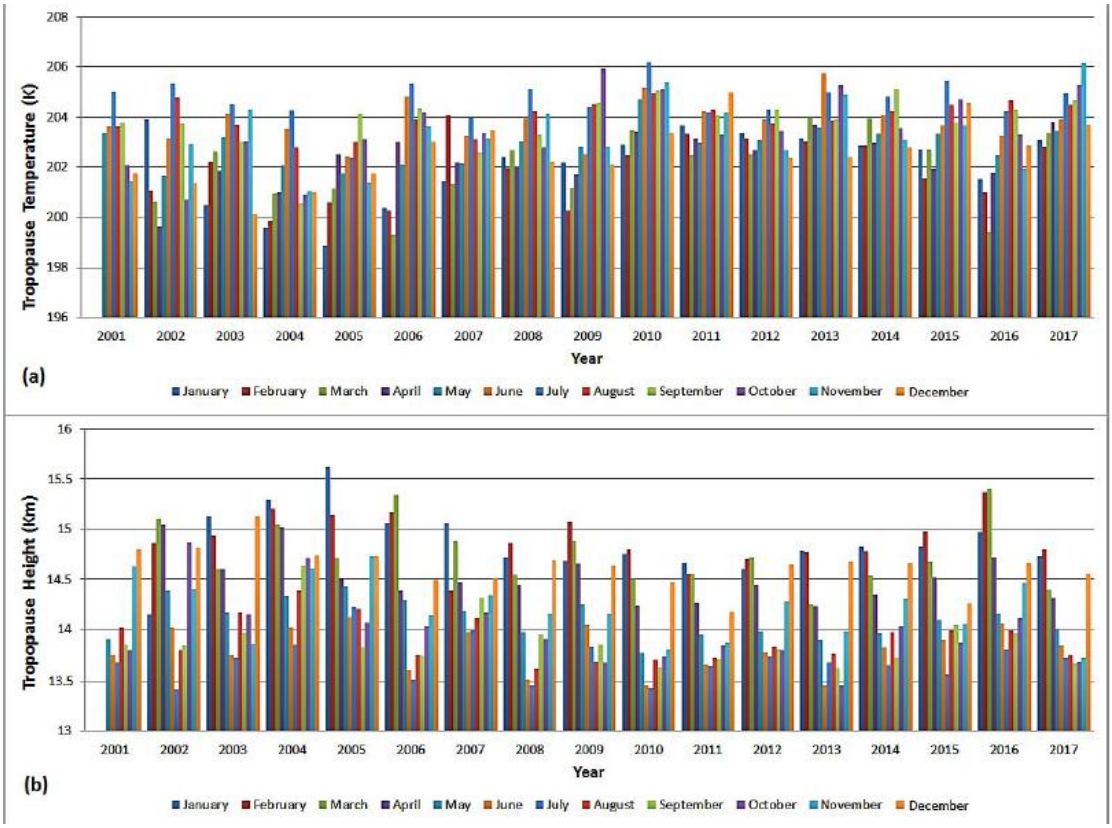

Source: The Author (2018).

4.3 SPATIO-TEMPORAL VARIATION

As discussed earlier, the tropopause parameters exhibit a strong latitudinal dependence. Feng, Fu, & Xiao, (2012), using radiosonde data between 1965 - 2004 presents the tropopause with average height ranging from 16.2km in the equatorial zone to 8.5km in the poles. The tropopause height estimated by the GNSS-RO data for the tropical zone (at the equator) is approximately 17km and at latitudes near 8km poles (RIECKH et al., 2014). Fig. 11 shows the tropopause behavior in relation to the latitudinal zones in SA for the year 2008 using COSMIC (green dots), GRACE (blue dots) and CHAMP (red dots). COSMIC provided the largest number of atmospheric profiles 58,548 while GRACE provided 3,130 and CHAMP 3,358, despite the difference in the amount of data, the three datasets showed the same behavior considering the latitudinal distribution.

Figure 11 - Height (a) and temperature (b) of the tropopause in relation to latitude variations derived from GNSS-RO observations during 2008.

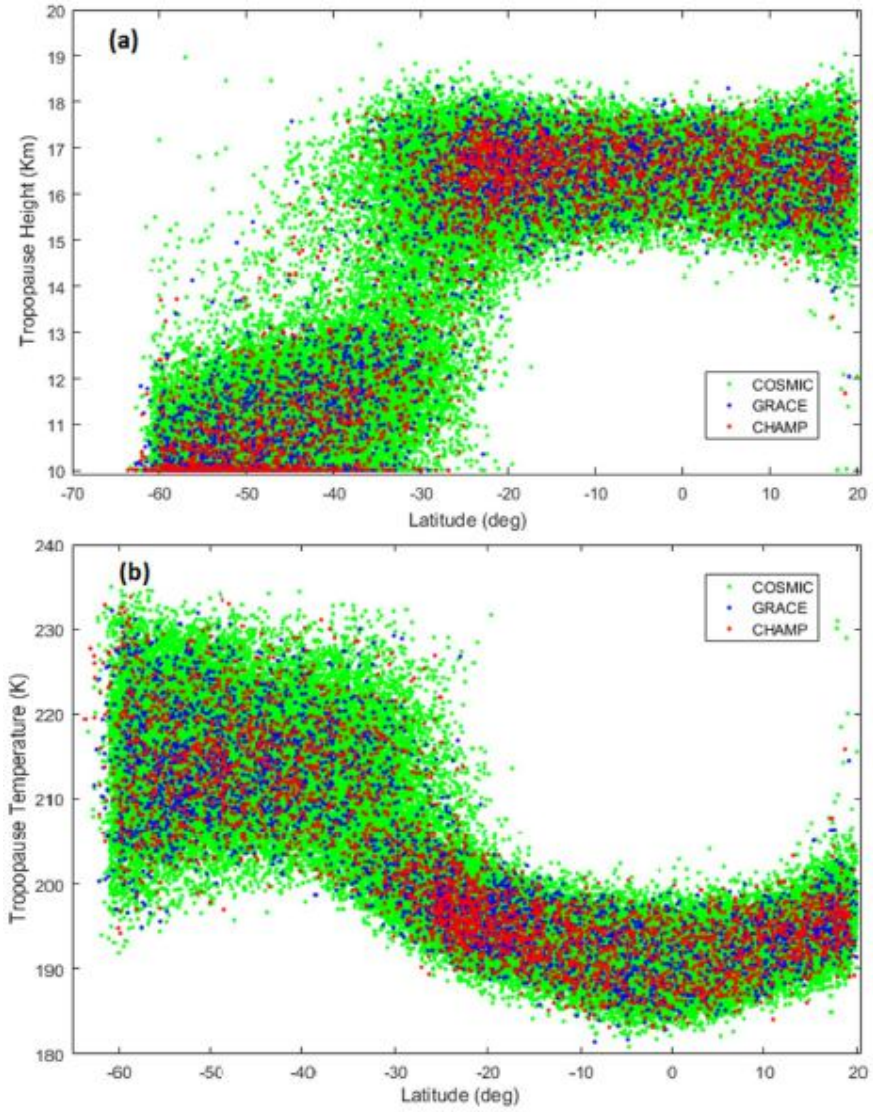

Source: The Author (2018).

Comparing Fig. 11a with the latitudinal division on table 2, it can be observed that for the tropical region (20°N - 20°S) the height tropopause varies between 15km and 18km with an average height of 16.64km and standard deviation of 0.39km. In the subtropical region (20°S - 40°S) is the highest heights variation, with values between 10km and 18km with an average of 14.50km and 0.92km of standard deviation. In the middle latitudes (40°S - 60°S) it is presented the lowest average for the tropopause height with 10.75km and 0.23km of standard deviation. The tropopause temperature (Fig. 11b) also showed a distribution based on the latitudinal

zones on Table 2, where the tropical region (20°N - 20°S) presented the lowest temperatures with a mean of 193,05K and 2,32K of standard deviation. The subtropical region (20°S - 40°S) presented a transition between the highest and lowest temperatures with a mean of 205.08K and 3.28K of standard deviation. The middle latitudes (40°S - 60°S) presented the highest temperatures with a mean of 215.15K and 2.78K standard deviation.

4.4 SEASONAL VARIATIONS

The tropopause behavior in the summer and winter seasons was studied in relation to the three GNSS-RO datasets (CHAMP, GRACE and COSMIC), using data from 2007 and 2008, period in which the data of the three missions are available. Fig. 12 shows the average height of the seasonal tropopause for the summer (January 2008 to March 2008), using CHAMP (Fig. 12a), GRACE (Fig. 12b) and COSMIC (Fig. 12c) for winter (July to September 2007), with CHAMP (Fig. 12d), GRACE (Fig. 12e) and COSMIC (Fig. 12f). During the summer, the tropopause height reaches the highest values in the Northwest region of SA and the lowest altitudes in the Southern region. The height average in the tropics (20°N - 20°S) is 16.88km with maximum values occurring between 17km and 18km, in medium latitudes (40°N - 60°S) the tropopause height average decreases to 10.84km. While in winter the tropopause height decreases, in the tropics (20°N - 20°S) the maximum values are concentrated between 16km and 17km with few occurrences above these values, the average in this region is 16.26km showing a seasonal height average decrease of 0.62km. In the middle latitudes (40°N - 60°S) the mean tropopause height decreases to 10.52km with values between 10km and 11km. In both summer and winter the tropopause height varies between the tropical region and the mid-latitudes approximately by 5km. Comparing the GNSS-RO results (CHAMP, GRACE and COSMIC), the three missions presented a similar structure for tropopause height, with higher heights for the summer than in winter. The CHAMP showed a slightly smaller tropopause height considering both summer and winter when compared to the others two datasets (GRACE and COSMIC).

Figure 12 - Seasonal distribution of tropopause height (km). Summer (2008): CHAMP (a) GRACE (b) and COSMIC (c), for winter (2007): CHAMP (d) GRACE (e) and COSMIC (f).

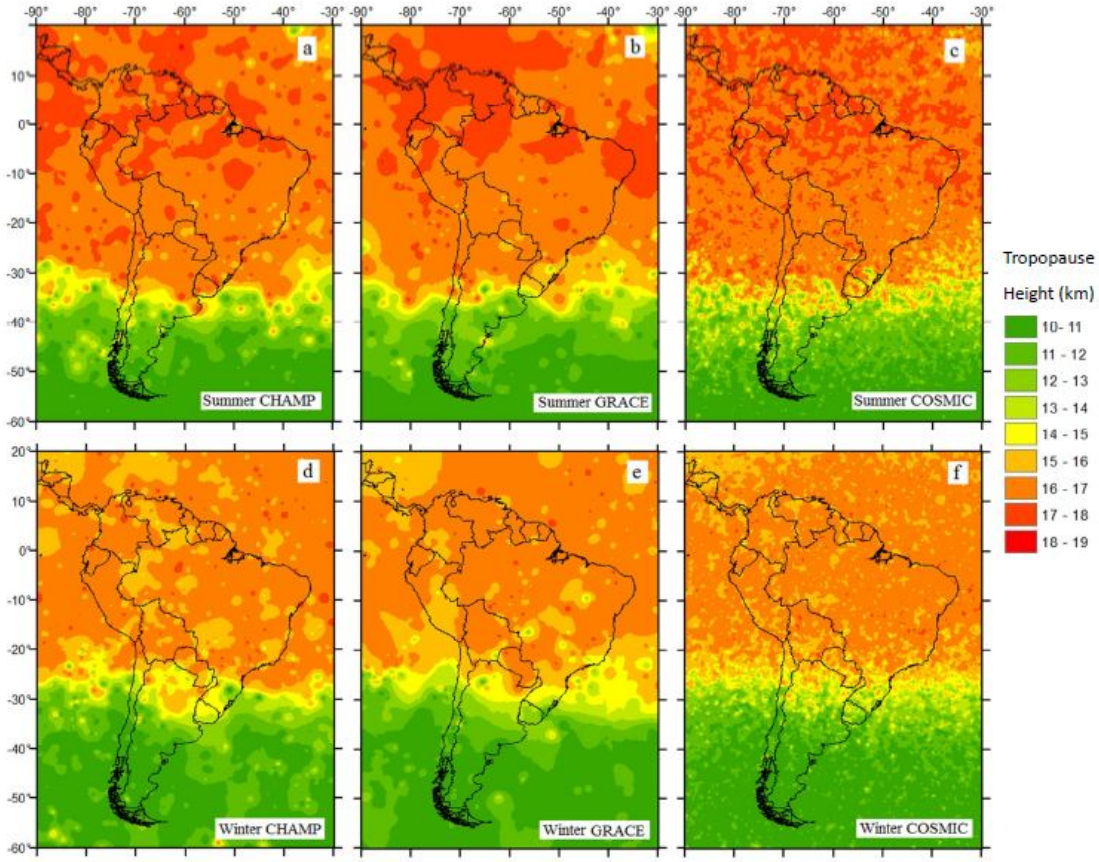

Source: The Author (2018).

Figure 13 shows the results for tropopause temperatures using GNSS-RO data between 2007 and 2008, summer (2008) and winter (2007) for CHAMP (Fig. 13a, 13d), GRACE (Fig. 13b, 13e) and COSMIC (Fig. 13c, 13f). The three datasets showed a similar tropopause temperature distribution. The summer temperatures (January - March) in the tropical region (20°N - 20°S) are lower than those of winter (July - September), this could be explained by the annual temperature cycle in this region presented by Reid & Gage, (1981) that using radiosonde data found temperatures on average 5K lower in January compared to August. When comparing the three missions it is possible to notice that COSMIC presented the highest temperatures, for summer and winter compared with CHAMP and GRACE.

Figure 13 - Seasonal distribution of tropopause temperature (k). Summer (2008): CHAMP (a) GRACE (b) and COSMIC (c), for winter (2007): CHAMP (d) GRACE (e) and COSMIC (f).

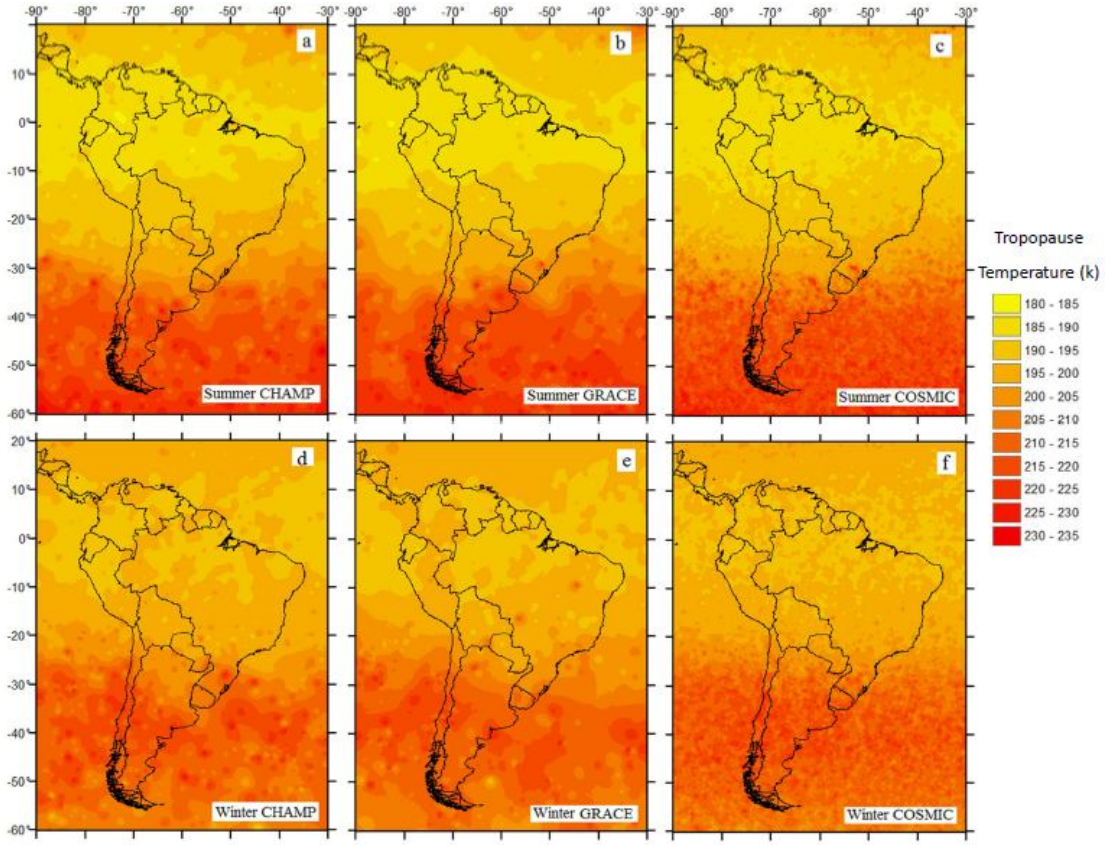

Source: The Author (2018).

4.5 TREND ANALYSIS

The temporal trend for tropopause height and temperature were investigated using, the tropopause height and temperature (Fig. 14) monthly anomalies time series which were evaluated by subtracting the annual cycle from each individual monthly average, this was done to remove the cyclical trend effect on the data. The trend and its respective standard error at ± 2-sigma significance level were calculated according to Karl et al., (2006).

Figure 14 - Tropopause height and temperature anomalies estimated from CHAMP, GRACE and COSMIC data between 2001 to 2017.

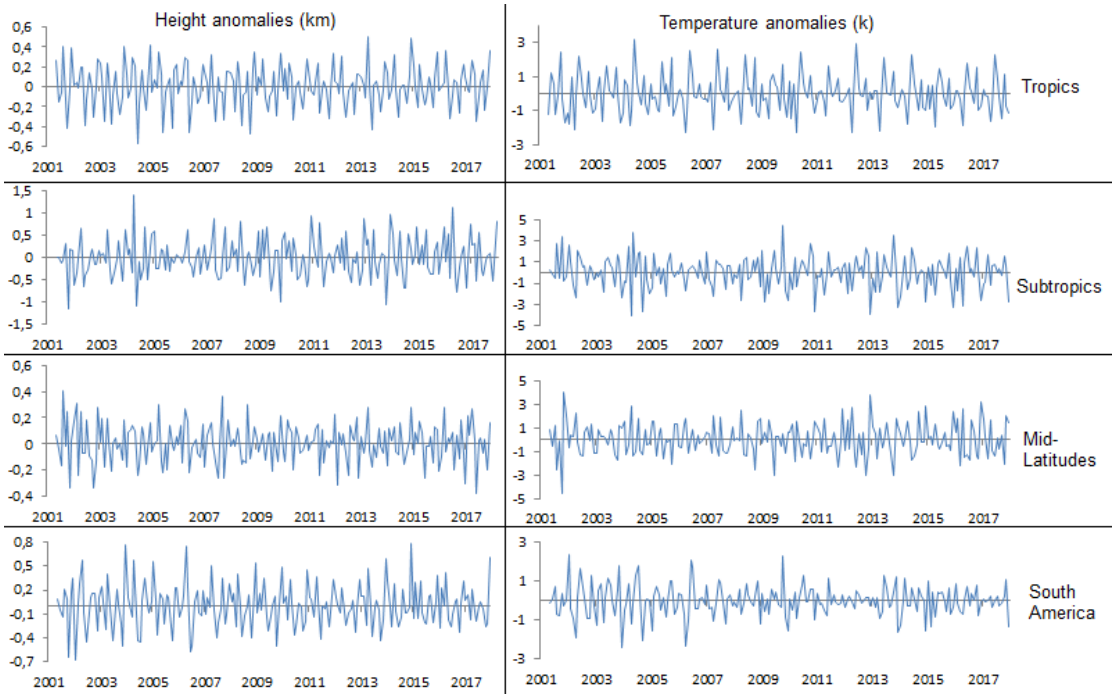

Source: The Author (2018).

The time series (2001 to 2017) trends of height and temperature anomalies estimated are summarized on Table 3. The tropopause height trend over South America is presented in m/decade and the temperature in k/decade, the linear regression adjusted trend faced an tropopause height increase of 13.450m/dec with a decrease of -0.021K/dec in temperature. Analyzing the SA latitudinal regions, the tropics and subtropics presented an upward tendency to the tropopause height with values of 8.734m/dec and 42.884m/dec and temperature descending with -0.019K/dec and -0.202K/dec, respectively. Only the middle latitudes region presented the tropopause height with -6.442m/dec, with is an negative tendency and an temperature increase of 0.006K/dec.

Table 3 - Trends in tropopause height and temperature in South America, estimated by CHAMP, GRACE and COSMIC between 2001 and 2017.

Zone	Height (m/dec)	Temperature (K/dec)
Tropics	8.734 ± 0.523	-0.019 ± 0.003
Subtropics	42.884 ± 1.102	-0.202 ± 0.004
Mid-latitudes	-6.442 ± 0.377	0.006 ± 0.003
South America	13.450 ± 0.677	-0.021 ± 0.002

Source: The Author (2018).

Seidel & Randel, (2006) presented a global tropopause study using radiosonde data between 1980 until 2004 with the tropopause height ascending trend estimated by 64 ± 21m/dec with a temperature decrease of 0.41 ± 0.09K/dec. The subtropics in the southern hemisphere being considered the region indicating the highest tropopause height increase of 121m/dec and 0.78K/dec. Although the trend results are lower than those estimated by Seidel & Randel, (2006), the results are showing agreement, since both represents an increasing tendency, being also in the subtropical region the greater tendency for tropopause height (42.884m/dec) and temperature (-0.202K/dec). However the main difference is in the middle latitudes region where Seidel & Randel, (2006) presented an upward tendency to the tropopause height and this study was found a tropopause height decrease.

The global study for tropopause height based on CHAMP data (May 2001 to December 2007, 80 months) Schmidt et al., (2008) found an tropopause height increase around 39 and 74m/dec, highlighting the subtropical regions where the most significant increases occurred, only the tropics and middle latitudes regions presented a negative tendency for tropopause height in those methods used. For this study, 13.450m/dec were found for the tropopause height demonstrating an increase in the SA that is in accordance with the global trend by Schmidt et al., (2008). The results showed the middle-latitudes with a negative height trend (-6.442m/dec) while Schmidt et al., (2008) has a trend estimated of -24m/dec, although the values found are different the trend direction are the same in both studies. The main difference in this comparison is observed in the tropics where Schmidt et al., (2008) estimated a decrease in the tropopause height and the current results showed an upward trend for this region.

There are several studies reporting tropopause regional changes e.g., Khandu et al., (2011) presented a trend for Australia tropopause height and temperature using GNSS-RO (2001 to 2008), with an upward estimate 7.2m/dec with only the middle-latitudes with a negative height trend. In this study, the trend of the height and temperature of the regional tropopause in SA presented the same sense of growth found by Khandu et al., (2011), with tropics and subtropics with ascending values for height and temperature decreases in the tropopause, also only the middle-latitudes region occurring tropopause height decrease and temperature increase. This trend results corroborate with previous studies, although with lower values (13.450m/dec).

Figure 15 shows the tropopause height and temperature variation rate in South America, obtained from CHAMP, GRACE and COSMIC (May 2001 to December 2017), the tropopause height variations is expressed by km/year (Fig. 15a) and the tropopause temperature variations in K/year (Fig. 15b). The results of the two sets (height and temperature) showed an anti-correlation, for example, in the region where there is tropopause height increase it presents a decrease in temperature. A large part of South America, presented variations between 0 and 0.1km/year of tropopause height increase with a corresponding tropopause temperature decrease (0 to - 0.3K/year), which are much higher than the presented trends on Table 3, probably because the trends are calculated based on the seasonal mean of anomalies. In spite of presenting higher values than the trends, it could be concluded that the variation rates (Fig. 15a and 15b) are corroborating with the tendencies presented in Table 3, e.g., the region with the greatest increase in height tendency and highest temperature decrease of the tropopause is the subtropical (20°S - 20°N) and this can be visually noticed in Fig. 15.

Figure 15 - Tropopause height and temperature variation rate between May 2001 to December 2017.

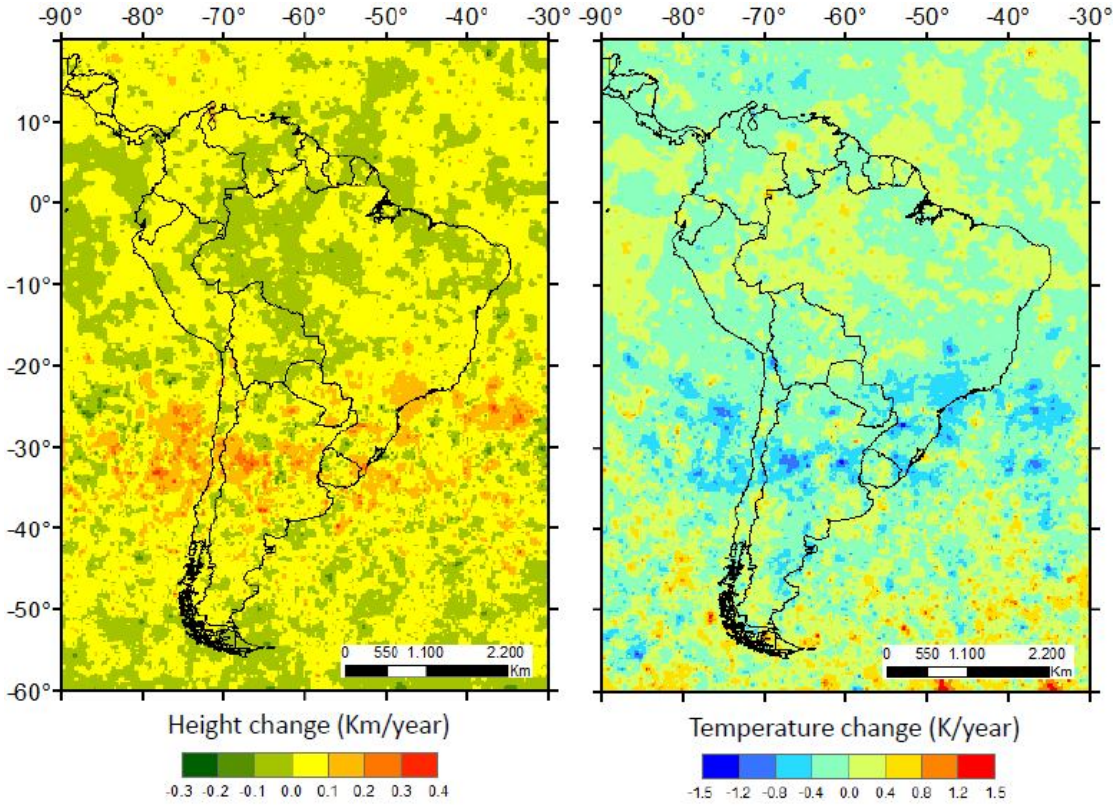

Source: The Author (2018).

The PCA was applied to the time series to analyze the correlation between teleconnections and tropopause (temperature and height) variability for SA, in this case the time series (May 2001 to December 2017) was divided into monthly grids in which the seasonal cycle was removed from each grid cell. Then the PCA was applied considering the deseasonalized time series to analyze the tropopause (temperature and height) spatial-temporal variability .Table 4 shows the variability rate explained by the three main EOFs obtained by PCA, the first two EOFs explain approximately 85% of the tropopause temperature and height variability.

Table.4 - The variability explained by the three main EOFs obtained by the PCA applied to the height and temperature anomalies of the tropopause.

	Temperature (%)	Height(%)
EOF1	71.58	54.37
EOF2	14.74	31.03
EOF3	7.92	8.26

Source: The Author (2018).

Figure 16 shows the spatial distribution of the 2 main EOFs for temperature, the first EOF (Fig. 16a) presents 71.57% of the variability with values between -4.2K and 6.5K, the tropical region presents almost uniform negative temperature variability, the subtropical region dominates the negative variability with the lowest values of temperature, while in the middle latitudes the variability is positive and increasing in the direction of the lower latitudes, this behavior resembles the rates of variation observed in Fig. 15b.

Figure 16 - The first two EOFs of tropopause temperature (K) anomalies based on GNSS-RO data for SA.

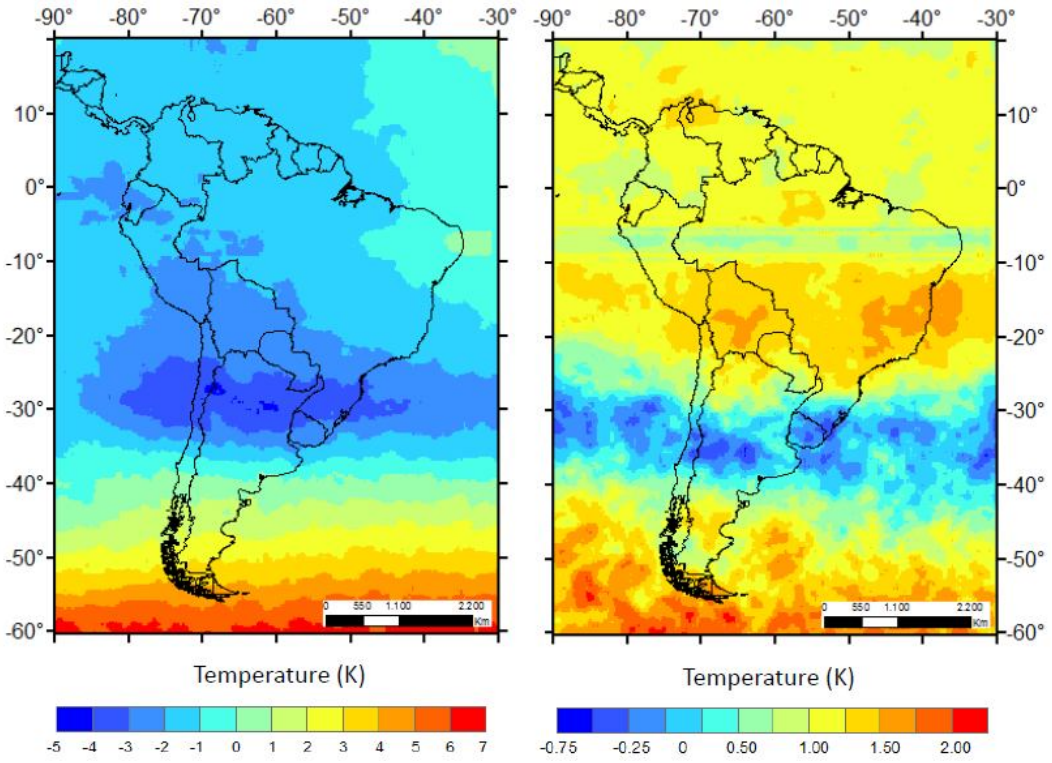

Source: The Author (2018).

The second temperature EOF in Fig. 16b explains an variability of 14.74% with values between -0.62K and 2.25K, the spatial distribution in the subtropical region and of the average latitudes resembles that observed in EOF1, however the EOF2, explains a positive variability in the tropical region, different from that one explained in EOF1, this is because each EOF is the result of a distinct function applied to the data, as in that region there are positive and negative rates (Fig. 15b), the EOF1 presented variability negative while the EOF2 presented positive, but since EOF1 explains 71.58% of the variability of the data, the negative variability is the dominant in the time series.

The EOFs for the tropopause height are shown in Fig. 17, the first EOF (Fig. 17a) explains 54.37% of the tropopause height variability, it is highlighted the subtropical region with greater positive variability, similar to the behavior of Fig. 15a for tropopause height annual rate variation. The second EOF explains 31.03% of the variability (Fig. 17b) and presents an opposite behavior to the EFO1 explaining the negative anomalies in the subtropical region.

Figure 17 - The first two EOFs of tropopause height (Km) anomalies based on GNSS-RO data for SA.

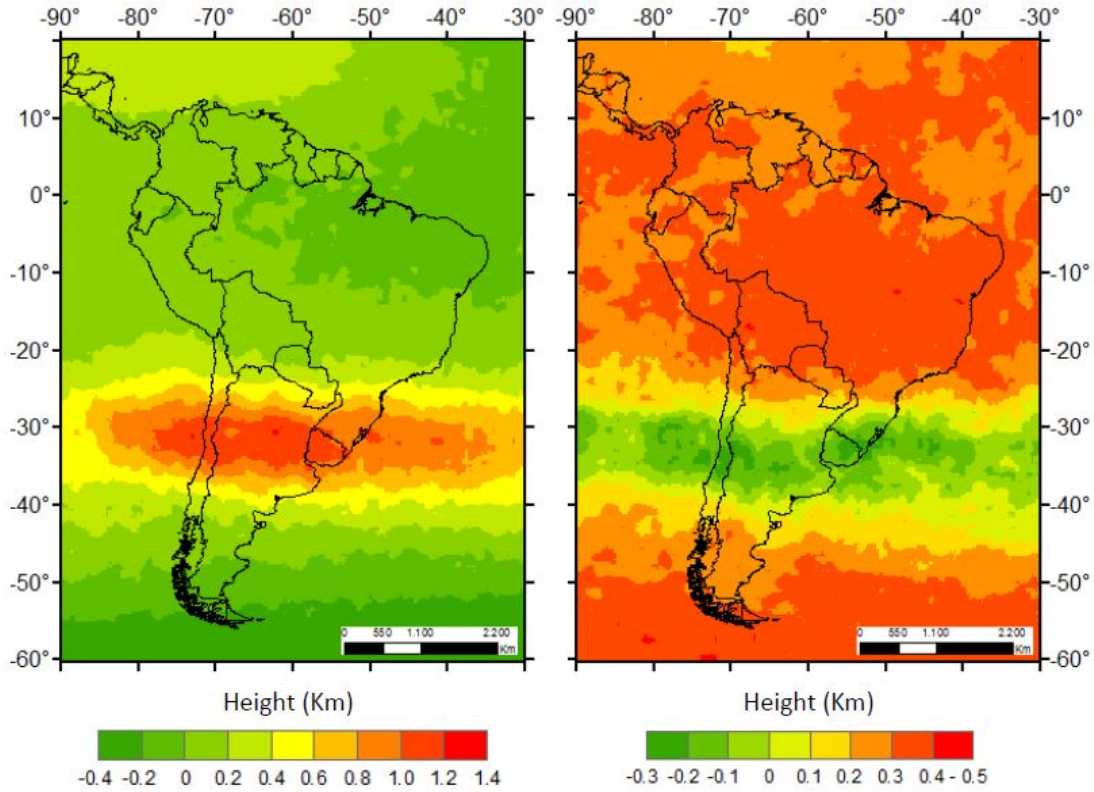

Source: The Author (2018).

The PCs, the main component of each EOFs, represent how the variability obtained by orthogonal spatial functions behaves throughout the time series. Table 5 presents the Pearson correlation between the PCs obtained from their respective EOFs and the ocean-atmospheric indexes. For the temperature, PC1 obtained from EOF1 representing 71.58% of the data variability over the time series, presented a significant 0.60 correlation with ENSO phenomenon through the ENSO 1+2 index. At the tropopause height, PC1 was obtained from the EOF1, which represents 54.37% of the height variability with a correlation of 0.52 with ENSO phenomena through the ENSO 1+2 index. The other ones indexes presented low correlation as can be followed in table 5. In order to demonstrate the influence of the ENSO phenomenon on the tropopause, Fig. 18 shows the temporal distribution of the monthly mean height and temperature anomalies and the ENSO Niño 1+2 index for SA between May 2001 and December 2017.

Table 5 - Pearson's correlation between tropopause height and temperature anomalies and the ocean-atmospheric indexes.

		QBO	Niño 3.4	Niño 1+2	TNA	TSA
Height	PC1	0.11	-0.21	0.52	-0.10	0.09
	PC2	0.03	0.07	-0.17	0.07	0.04
	PC3	0.09	-0.07	0.31	-0.23	0.07
	PC4	-0.04	0.19	0.06	0.00	0.07
Temperature	PC1	0.11	-0.18	0.60	-0.14	0.08
	PC2	-0.07	0.08	0.07	-0.10	-0.04
	PC3	0.06	-0.17	-0.15	0.08	-0.10
	PC4	-0.06	-0.17	-0.38	0.29	-0.13

Source: The Author (2018).

Figure 18 - Temporal distribution of the mean height and temperature anomalies and the ENSO (Niño 1+2) for the period of May 2001 to December 2017.

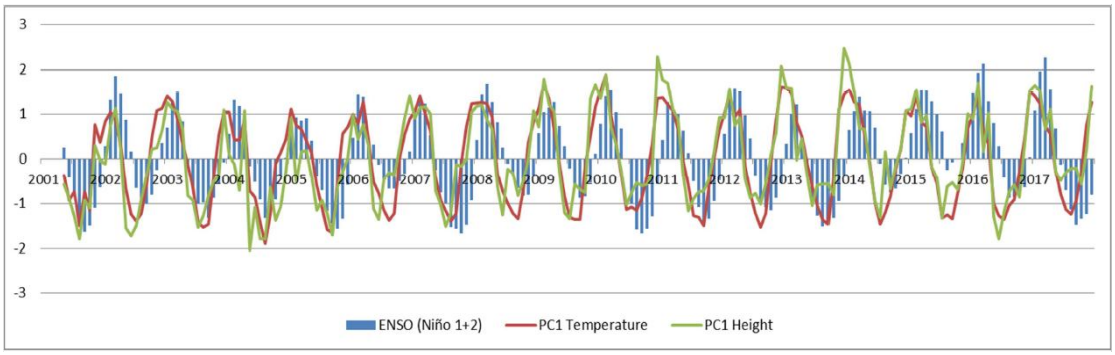

Source: The Author (2018).

5 CONCLUSIONS AND RECOMMENDATIONS

This study indicated that the spatial (Fig. 5) and temporal (Fig. 6) distribution of GNSS-RO over South America provides a significant amount of data that provides an excellent opportunity to monitor the tropopause over South America. With GNSS-RO profiles found within a range of 100km and 3 hours from the nearest radiosonde measurements, it has been shown that GNSS-RO temperature profiles agree with radiosonde measurements with bias than 1 ± 2K in the region of tropopause. The best agreements are seen between 10km and 25km in height with measurements with precision greater than 0.6 ± 2K presented by COSMIC. Thus, the GNSS-RO atmospheric profiles of the temperatures and heights of the tropopause match well with those of the radiosonde measurements and may be suitable for use in regional climate change analysis.

The regional tropopause' structure (height and temperature trends) was analyzed using 200 months (May 2001 to December 2017) of CHAMP, GRACE and COSMIC data, to date the largest time series available. This study shows a growing trend at the height of the regional tropopause for South America of 13,450m/dec with a corresponding temperature decrease of -0.021K/dec (see, table 3). This value is smaller than the increasing estimate of the global tropopause height found Schmidt et al., (2008) and Seidel & Randel, (2006), but it is necessary to consider the use of different data sets and time scale. Despite the difference in values, the results corroborating by indicating an tropopause height trend with a decreasing trend of temperature throughout the study period. In the study case showed by Khandu et al., (2011), although a different tropopause region (Australia) is approached, the results obtained concur with the same direction for the tropopause (height and temperature) trend. The analysis of the tropopause over South America provides evidence for regional warming trends.

The PCA applied in height and temperature anomalies of the tropopause for SA showed a significant correlation of 0.60 for temperature and 0.52 for height with the atmospheric phenomenon ENSO through the ocean-atmospheric index ENSO Niño 1+2. This result is an indicator of how global teleconnection mechanisms, in this case the ENSO cold and hot phases, are correlated with tropopause variability in SA. The Atlantic Ocean indexes (TSA and TNA) and QBO presented a low correlation

with the height and temperature anomalies of the tropopause for SA, probably because these indexes are associated with the tropical region and the greater variability of the SA data occurs in the subtropical region and middle latitudes, to establish a more detailed analysis of this correlation, in future studies it is recommended to analyze this correlation in specific regions of SA.

The literature argues that the tropopause height trends are a useful climate change indicative associated with troposphere and stratosphere temperature variations. Therefore, having the ability to accurately monitor the tropopause trends in a suitable spatial and temporal resolution has the potential to provide monitoring for regional warming. This study provides the ability to perform a tropopause monitoring using radiosonde observations records of and particularly GNSS-RO.

REFERENCES

ANDREOLI, R.V.; KAYANO, M.T.; GUEDES, R.L.; OYAMA, M.D.; & ALVES, M.A.S., A influência da temperatura da superfície do mar dos Oceanos Pacífico e Atlântico na variabilidade de precipitação em Fortaleza. **Revista Brasileira de Meteorologia**, v. 19, n. 3, p. 337-344, 2004.

ANGELL, J.K.; KORSHOVER, J., Quasi-biennial variations in temperature, total ozone, and tropopause height. **Journal of the Atmospheric Sciences**, v. 21, n. 5, p. 479-492, 1964.

ANTHES, R.A.; ECTOR, D.; HUNT, D.C.; KUO, Y.H.; ROCKEN, C.; SCHREINER, W.S.; SOKOLOVSKIY, S.V.; SYNDERGAARD, S.; WEE, T.K.; ZENG, Z.; BERNHARDT, P.A.; DYMOND, K.F.; CHEN, Y.; LIU, H.; MANNING, K.; RANDEL, W.J.; TRENBERTH, K.E.; CUCURULL, L.; HEALY, S.B.; HO, S.P.; MCCORMICK, C.; MEEHAN, T.K.; THOMPSON, D.C.; & YEN, N.L.; The COSMIC/FORMOSAT-3 mission: Early results. **Bulletin of the American Meteorological Society**, v. 89, n. 3, p. 313-334, 2008.

AWANGE, J.L.; GRAFAREND, E.W. **Solving algebraic computational problems in geodesy and geoinformatics**. Berlin etc.: Springer, 2005.

BALDWIN, M.P.; GRAY, L.J.; DUNKERTON, T.J.; HAMILTON, K.; HAYNES, P.H.; RANDEL, W.J.; HOLTON, J.R.; ALEXANDER, M.J.; HIROTA, I.; HORINOUCHI, T.; JONES, D.B.A.; KINNERSLEY, J.S.; MARQUARDT, C.; SATO, K.; & TAKAHASHI, M., The quasi-biennial oscillation. **Reviews of Geophysics**, v. 39, n. 2, p. 179-229, 2001.

CAVALCANTI, I.F. de A.; AMBRIZZI, T., Teleconexões e suas influências no Brasil. **Tempo e clima no Brasil**, 2009.

ESPINOZA, J.C.; RONCHAIL, J.; GUYOT, J.L.; COCHONNEAU, G.; NAZIANO, F.; LAVADO, W.; OLIVEIRA, E.; POMBOSA, R.; AND VAUCHEL, P., Spatio-temporal rainfall variability in the Amazon basin countries (Brazil, Peru, Bolivia, Colombia, and Ecuador). **International Journal of Climatology: A Journal of the Royal Meteorological Society**, v. 29, n. 11, p. 1574-1594, 2009.

ESPINOZA, J.C.; LENGAIGNE, M.; RONCHAIL, J.; & JANICOT, S., Large-scale circulation patterns and related rainfall in the Amazon Basin: a neuronal networks approach. **Climate dynamics**, v. 38, n. 1-2, p. 121-140, 2012.

ESPINOZA, J.C.; RONCHAIL J.; FRAPPART F.; LAVADO W.; SANTINI W.; & GUYOT, J.L., The major floods in the Amazonas River and tributaries (western

Amazon basin) during the 1970–2012 period: A focus on the 2012 flood. **Journal of Hydrometeorology**, v. 14, n. 3, p. 1000-1008, 2013.

FENG, S., FU, Y., & XIAO, Q., Trends in the global tropopause thickness revealed by radiosondes. **Geophysical Research Letters**, v. 39, n. 20, 2012.

FONG, C.J.; SHIAU, W.T.; LIN, C.T.; KUO, T.C.; CHU, C.H.; YANG, S.K.; ... & CHI, S., Constellation deployment for the FORMOSAT-3/COSMIC mission. **IEEE Transactions on Geoscience and Remote Sensing**, v. 46, n. 11, p. 3367-3379, 2008.

GETTELMAN, A.; RANDEL, W.J.; MASSIE, S.; WU, F.; READ, W.G.; & RUSSELL III, J.M., El Nino as a natural experiment for studying the tropical tropopause region. **Journal of climate**, v. 14, n. 16, p. 3375-3392, 2001.

GIANNINI, A.; SARAVANAN, R.; & CHANG, P., The preconditioning role of tropical Atlantic variability in the development of the ENSO teleconnection: Implications for the prediction of Nordeste rainfall. **Climate Dynamics**, v. 22, n. 8, p. 839-855, 2004.

HOLZSCHUH, M.L.; SAPUCCI, L.F.; MONICO, J.F.G., Avaliação de perfis atmosféricos de rádio ocultação GPS do satélite CHAMP sobre a América do Sul. **Revista Brasileira de Meteorologia**, p. 147-155, 2010.

JIN, S.; CARDELLACH, E.; XIE, F., **GNSS remote sensing.** Dordrecht: Springer, 2014.

KARL, T.R.; HASSOL, S.J.; MILLER, C.D.; & MURRAY, W.L., Temperature Trends in the Lower Atmosphere: Steps for Understanding and Reconciling Differences. **US Climate Change Science Program and the Subcommittee on Global Change Research**, Washington, D. C. 2006

KHANDU, K.; AWANGE, J.L.; WICKERT, J.; SCHMIDT, T.; SHARIFI, M.A.; HECK, B.; FLEMING, K., GNSS remote sensing of the Australian tropopause. **Climatic Change**, 105, 597–618. 2011.

KHANDU, K.; AWANGE, J.L; & FOROOTAN, E., Interannual variability of temperature in the UTLS region over Ganges--Brahmaputra--Meghna river basin based on COSMIC GNSS RO data. **Atmospheric Measurement Techniques**, 9, 1685-1699. 2016.

LEWIS, S.L.; BRANDO, P.M.; PHILLIPS, O.L.; VAN DER HEIJDEN, G.M.F.; & NEPSTAD, D., The 2010 amazon drought. **Science**, v. 331, n. 6017, p. 554-554,

2011.

MAGRIN, G.O.; MARENGO, J.A.; BOULANGER, J.P.; BUCKERIDGE, M.S.; CASTELLANOS, E.; POVEDA, G.; SCARANO, F.R.; & VICUÑA, S., **Central and South America in Climate Change 2014: Impacts, Adaptation, and Vulnerability**. Part B: Regional Aspects. Contribution of Working Group II to the Fifth Assessment Report of the Intergovernmental Panel of Climate Change (eds. Barros, VR et al.), 1499-1566, 2014.

MARENGO, J.A.; NOBRE, C.A.; TOMASELLA, J.; OYAMA, M.D.; OLIVEIRA, G.S.; OLIVEIRA, R.; CAMARGO, H.; ALVES, L.M.; & BROWN, I.F., The drought of Amazonia in 2005. **Journal of climate**, v. 21, n. 3, p. 495-516, 2008.

MARENGO, J.A.; TOMASELLA, J.; ALVES, L.M.; SOARES, W.R.; & RODRIGUEZ, D.A., The drought of 2010 in the context of historical droughts in the Amazon region. **Geophysical Research Letters**, v. 38, n. 12, 2011.

MARENGO, J.A.; PABÓN, J.D.; DÍAZ, A.; ROSAS, G.; ÁVALOS, G.; MONTEALEGRE, E.; & ROJAS, M., **Climate change: evidence and future scenarios for the Andean region. Climate change and biodiversity in the tropical Andes. IAI-SCOPE-UNESCO, Paris, France**, p. 110-127, 2011b.

MARENGO, J.A.; TOMASELLA, J.; SOARES, W. R.; ALVES, L.M.; & NOBRE, C.A.; Extreme climatic events in the Amazon basin. **Theoretical and Applied Climatology**, v. 107, n. 1-2, p. 73-85, 2012.

MARENGO, J.A.; ALVES, L.M.; SOARES, W.R.; RODRIGUEZ, D.A.; CAMARGO, H.; RIVEROS, M.P.; & PABLÓ, A.D., Two contrasting severe seasonal extremes in tropical South America in 2012: flood in Amazonia and drought in northeast Brazil. **Journal of climate**, v. 26, n. 22, p. 9137-9154, 2013.

MELBOURNE, W.G.; DAVIS, E.S.; DUNCAN, C.B.; HAJJ, G.A.; HARDY, K.R.; KURSINSKI, E.R.; MEEHAN, T.K.; YOUNG, L.E.; YUNCK, T.P., **The application of spaceborne GPS to atmospheric limb sounding and global change monitoring**. 1994.

MOURA, A.D., & SHUKLA, J., On the dynamics of droughts in northeast Brazil: Observations, theory and numerical experiments with a general circulation model. **Journal of the atmospheric sciences**, v. 38, n. 12, p. 2653-2675, 1981.

OLIVEIRA, F.P.; AMORIM, H.S.; DERECZYNSKI, C. P. Investigating the atmosphere with data obtained by radiosondes. **Revista Brasileira de Ensino de Física**, v. 40,

n. 3, 2018.

PREISENDORFER, R. Ä. N. Ü. **Principal component analysis in meteorology and oceanography**. Elsevier Sci. Publ., v. 17, p. 425, 1988.

RANDEL, W.J.; WU, F.; & GAFFEN, D.J., Interannual variability of the tropical tropopause derived from radiosonde data and NCEP reanalyses. **Journal of Geophysical Research: Atmospheres**, v. 105, n. D12, p. 15509-15523, 2000.

REID, G.C., & GAGE, K.S., On the annual variation in height of the tropical tropopause. **Journal of the Atmospheric Sciences**, v. 38, n. 9, p. 1928-1938, 1981.

REID, G.C., & GAGE, K.S., Interannual variations in the height of the tropical tropopause. **Journal of Geophysical Research: Atmospheres**, v. 90, n. D3, p. 5629-5635, 1985.

RIECKH, T.; SCHERLLIN-PIRSCHER, B.; LADSTÄDTER, F.; & FOELSCHE, U., Characteristics of tropopause parameters as observed with GPS radio occultation. **Atmospheric Measurement Techniques**, v. 7, n. 11, p. 3947-3958, 2014.

RUSTICUCCI, M.; TENCER, B., Observed changes in return values of annual temperature extremes over Argentina. **Journal of Climate**, v. 21, n. 21, p. 5455-5467, 2008.

SANTER, B.D.; WEHNER, M.F.; WIGLEY, T.M.L.; SAUSEN, R.;, MEEHL, G.A.; TAYLOR, K.E.; AMMANN, C.; ARBLASTER, J.; WASHINGTON, W.M.; BOYLE, J.S.; & BRÜGGEMANN, W., Contributions of anthropogenic and natural forcing to recent tropopause height changes. **Science**, v. 301, n. 5632, p. 479-483, 2003.

SANTER, B.D.; WIGLEY, T.M.; SIMMONS, A.J.; KALLBERG, P.W.; KELLY, G.A.; UPPALA, S.M.; AMMANN C.; BOYLE J.S.; BRÜGGEMANN, W.; DOUTRIAUX, C.; FIORINO, M.; MEARS C.; MEEHL G.A.; SAUSEN R.; TAYLOR K.E.; WASHINGTON W.M.; WEHNER M. F.; WENTZ F.J., Identification of anthropogenic climate change using a second-generation reanalysis. **Journal of Geophysical Research: Atmospheres**, v. 109, n. D21, 2004.

DOS SANTOS, C.A.C.; & DE BRITO, J.I.B., Análise dos índices de extremos para o semi-árido do Brasil e suas relações com TSM e IVDN. **Revista Brasileira de Meteorologia**, v. 22, n. 3, p. 303-312, 2007.

SATYAMURTY, P.; DA COSTA, C.P.W.; MANZI, A.O.; & CANDIDO, L.A., A quick look at the 2012 record flood in the Amazon Basin. **Geophysical Research Letters**,

v. 40, n. 7, p. 1396-1401, 2013

SCHMIDT, T.; WICKERT, J.; BEYERLE, G.; & HEISE, S., Global tropopause height trends estimated from GPS radio occultation data. **Geophysical Research Letters**, v. 35, n. 11, 2008.

SEIDEL, D.J.; & RANDEL, W.J. Variability and trends in the global tropopause estimated from radiosonde data. **Journal of Geophysical Research: Atmospheres**, v. 111, n. D21, 2006.

TAPLEY, B.D.; BETTADPUR, S.; WATKINS, M.; & REIGBER, C. The gravity recovery and climate experiment: Mission overview and early results. **Geophysical Research Letters**, v. 31, n. 9, 2004.

TRENBERTH, K.E. The definition of el nino. **Bulletin of the American Meteorological Society**, v. 78, n. 12, p. 2771-2778, 1997.

TRENBERTH, K.E., & STEPANIAK, D. P., Indices of el Niño evolution. **Journal of climate,** v. 14, n. 8, p. 1697-1701, 2001.

WICKERT, J.; REIGBER, C.; BEYERLE, G.; KÖNIG, R.; MARQUARDT, C.; SCHMIDT, T.; GRUNWALD, L.; GALAS, R.; MEEHAN, T.K.; MELBOURNE, W.G.; HOCKE, K., Atmosphere sounding by GPS radio occultation: First results from CHAMP. **Geophysical research letters**, v. 28, n. 17, p. 3263-3266, 2001.

WICKERT, J.; SCHMIDT, T.; BEYERLE, G.; KÖNIG, R.; REIGBER, C.; & JAKOWSKI, N., The radio occultation experiment aboard CHAMP: Operational data analysis and validation of vertical atmospheric profiles. **Journal of the Meteorological Society of Japan**. Ser. II, v. 82, n. 1B, p. 381-395, 2004.

WICKERT, J., **Comparison of vertical refractivity and temperature profiles from CHAMP with radiosonde measurements**. Geoforschungszentrum, 2004b.

WICKERT, J.; BEYERLE, G.; KÖNIG, R.; HEISE, S.; GRUNWALDT, L.; MICHALAK, G.; REIGBER, C.H.; & SCHMIDT, T., GPS radio occultation with CHAMP and GRACE: A first look at a new and promising satellite configuration for global atmospheric sounding. **Annales Geophysicae**, 2005. p. 653-658.

WICKERT, J.; MICHALAK, G.; SCHMIDT, T.; BEYERLE, G.; CHENG, C.Z.; HEALY, S.B.; HEISE, S.; HUANG, C.Y.; JAKOWSKI, N.; KÖHLER, W.; MAYER, C., OFFILER, D.; OZAWA, E.; PAVELYEV, A.G.; ROTHACHER, M.; TAPLEY, B.; ARRAS, C.; GPS radio occultation: results from CHAMP, GRACE and FORMOSAT-3/COSMIC. **Terrestrial, Atmospheric and Oceanic Sciences**, v. 20, n. 1, 2009.

WMO, Meteorology. A Three-Dimensional Science: Second Session of the Commission for aerology. **WMO Bulletin**, v. 6, p. 134-138, 1957.